Marine Pollution Bulletin 184 (2022) 114161

Contents lists available at ScienceDirect

Marine Pollution Bulletin

journal homepage: www.elsevier.com/locate/marpolbul

Dissolved and particulate iron redox speciation during the LOHAFEX fertilization experiment

Luis M. Laglera [a,b,*,1], Hema Uskaikar [c,1], Christine Klaas [d], S. Wajih A. Naqvi [c], Dieter A. Wolf-Gladrow [d], Antonio Tovar-Sánchez [e]

[a] FI-TRACE, Departamento de Química, Universidad de las Islas Baleares, Palma, Balearic Islands 07122, Spain
[b] Laboratori Interdisciplinari sobre Canvi Climàtic, Universidad de las Islas Baleares, Palma, Balearic Islands 07122, Spain
[c] National Institute of Oceanography, Dona Paula, Goa, India
[d] Alfred Wegener Institute for Polar and Marine Research, Am Handelshafen 12, 27570 Bremerhaven, Germany
[e] Department of Ecology and Coastal Management, Andalusian Institute for Marine Science, ICMAN (CSIC), Campus Universitario Río San Pedro, Puerto Real, Cádiz, Spain

ARTICLE INFO

Keywords:
Iron ocean cycling
Iron redox speciation
Southern Ocean
Copepod grazing
Top-down trace element control

ABSTRACT

The redox speciation of iron was determined during the iron fertilization LOHAFEX and for the first time, the chemiluminescence assay of filtered and unfiltered samples was systematically compared. We hypothesize that higher chemiluminescence in unfiltered samples was caused by Fe(II) adsorbed onto biological particles. Dissolved and particulate Fe(II) increased in the mixed layer steadily 6-fold during the first two weeks and decreased back to initial levels by the end of LOHAFEX. Both Fe(II) forms did not show diel cycles downplaying the role of photoreduction. The chemiluminescence of unfiltered samples across the patch boundaries showed strong gradients, correlated significantly to biomass and the photosynthetic efficiency and were higher at night, indicative of a biological control. At 150 m deep, a secondary maximum of dissolved Fe(II) was associated with maxima of nitrite and ammonium despite high oxygen concentrations. We hypothesize that during LOHAFEX, iron redox speciation was mostly regulated by trophic interactions.

1. Introduction

Iron limitation of primary production is a common feature in vast areas of the ocean. Changes in iron concentration and bioavailability have the potential to modify biomass, CO_2 atmosphere-ocean fluxes, biological community structures, carbon sinking fluxes and many other processes of paramount ecological relevance (Assmy et al., 2007; Cooper et al., 1996; Kolber et al., 1994; Pollard et al., 2009). After 3 decades of intensive work, mostly linked to the GEOTRACES program (Anderson et al., 2014), we have a reasonable description of dissolved iron (DFe) concentrations and fluxes at a global scale (Moore and Braucher, 2008). However, there are still many uncertainties concerning iron organic and redox speciation, iron recycling and the favored biological uptake routes, including the extracellular redox processes that modulate Fe bioavailability (Morrissey and Bowler, 2012).

Although not universal, the reduced form of iron Fe(II) seems strongly favored during iron uptake by eukaryotic phytoplankton (Morrissey and Bowler, 2012) which actively reduce Fe(III) to Fe(II) as an acquisition strategy (Maldonado et al., 2001). In oxygen depleted waters, the low redox potential favors the formation and stability of highly soluble Fe(II) species (Stumm and Morgan, 1996). The highly insoluble Fe(III) is the thermodynamically stable species at the pH and oxygen concentrations of the ocean surface (Stumm and Morgan, 1996). Complexation with naturally occurring organic ligands and the formation of transitory Fe(II) enhances dissolved Fe (DFe) concentrations to the range between 10^{-10} to 10^{-9} M (Liu and Millero, 2002).

Both organically complexed and colloidal Fe(III) are reduced by various processes: ligand to metal charge transfer (LMCT), reaction with superoxide (O_2^-), reaction with cell surface reductases, and dark reduction in solution after reaction with reductant biological exudates and reductant dissolved organic matter (DOM) (Lee et al., 2017; Rose, 2012; Wells et al., 1991). The necessary information to ascertain the contribution of the different processes under natural conditions is still lacking. Recent studies have pointed to O_2^- as the key species in the reduction of

* Corresponding author at: FI-TRACE, Departamento de Química, Universidad de las Islas Baleares, Palma, Balearic Islands 07122, Spain.
E-mail address: luis.laglera@uib.es (L.M. Laglera).
[1] Laglera, L. M. and Uskaikar H. should be considered joint first authors.

https://doi.org/10.1016/j.marpolbul.2022.114161
Received 14 July 2022; Received in revised form 15 September 2022; Accepted 17 September 2022
Available online 27 September 2022

Fe(III) in the euphotic layer (Shaked and Rose, 2013). Accordingly, Fe (II) would be mainly formed after reaction with extracellular O_2^- formed by still not fully understood biological processes (Rose and Waite, 2005). This theory is supported by the fast reaction of O_2^- with any organic or inorganic form of Fe(III) (Rose, 2012). The dark formation of O_2^- is also possible from the oxidation of trace elements (e.g.: Cu) and some components of DOM (Rose, 2012), but the importance of dark O_2^- generation has not been evaluated yet.

Freshly formed Fe(II) is quickly oxidized by O_2 and reactive oxygen species (ROS), namely hydrogen peroxide (H_2O_2), hydroxyl radical ($OH\cdot$) and O_2^- (Gonzalez-Davila et al., 2005) formed through photochemical reactions of O_2 and colored dissolved organic matter (CDOM). Many DOM components, including algae exudates, extend the half-life of dissolved Fe(II) (thereafter "DFe(II)") in seawater possibly through complexation (González et al., 2014; Hopwood et al., 2020; Rose and Waite, 2003a; Rose and Waite, 2003b; Santana-Casiano et al., 2000). The change of DFe(II) oxidation rates after removal of all ligands by UV digestion is strong indirect evidence of the natural existence of Fe(II) specific ligands in the ocean (Roy et al., 2008).

DFe(II) concentrations are the result of the balance between the reduction and oxidation processes mentioned above. Typical DFe(II) profiles in ocean waters are characterized by higher concentrations in the euphotic layer. However, DFe(II) secondary maxima in deeper waters (100–300 m) with lower oxygen concentrations have been often found associated with nitrite (NO_2^-) maxima (Kondo and Moffett, 2013).

The commonly accepted paradigm is that, since many Fe(III) reduction reactions require the effect of solar radiation, DFe(II) concentrations show a daily period that peaks around midday and reaches a minimum at nighttime (Bowie et al., 2002; Rijkenberg et al., 2005; Waite et al., 1995), notwithstanding the fact that Fe(II) oxidation is accelerated during daytime by (photo)formation of ROS. However, many previous studies have also shown, against the referred paradigm, steady surface DFe(II) concentrations throughout a day/night cycle (Croot et al., 2001; Hansard et al., 2009; Hopwood et al., 2014; Sarthou et al., 2011).

Appropriate interpretation of Fe(II) concentrations determined during field surveys must, therefore, consider that iron redox speciation is a very dynamic process with strong spatial and temporal variations. DFe (II) has usually been determined in oceanic surveys or in mesocosm experiments. Data on the temporal dynamics of iron redox speciation in a specific water mass are scant and were mostly acquired during ocean iron fertilization (OIF) experiments (Croot et al., 2008; Croot et al., 2001; Croot et al., 2005; Roy et al., 2008). In these studies, DFe(II) concentrations remained high and contributed significantly to DFe concentrations days after the fertilization. This was despite the short dark half-life (from a few minutes to 2 h) of DFe(II) in seawater (Croot and Laan, 2002; King et al., 1995; Shaked, 2008). The interpretation put forward was that long stabilization was due to complexation with uncharacterized Fe(II) specific ligands mentioned above. However, controlled laboratory studies with known components of oceanic DOM never reached Fe(II) half-lives longer than few hours with measurable night DFe(II) concentrations. These results suggest that unknown Fe(III) reduction processes, attributed to extracellular enzymatic reduction (Croot et al., 2001), continuously generate Fe(II).

To the best of our knowledge, there has been no previous field study comparing Fe(II) concentrations in the water column before and after filtration. Spectrophotometric and chemiluminescence Fe(II) field studies have always been carried out in filtered samples with only one exception (Sarthou et al., 2011). In order to minimize the period between Niskin bottles closure and analysis, Sarthou and coauthors only analyzed unfiltered samples. They considered that their Fe(II) concentrations were valid surrogates to DFe(II) concentrations and reported Fe (II) concentrations in the ML waters of the Atlantic Sector of the Southern Ocean ranging from <detection limit of 0.009 nM to 0.125 nM. The approach seemed validated by the range of contribution of Fe(II) to DFe (39 to 63 %), ranges inside previously published DFe(II) to DFe ratios. The presence of Fe(II) in colloidal and particulate matter in the ocean has been scarcely discussed. A prior study on the redox speciation of iron in organic-mineral colloids collected in oxic surface Southern Ocean waters found that 12 % of the particles analyzed by X-ray spectromicroscopy presented Fe(II)/Fe(III) mixtures (von der Heyden et al., 2014). Addition of Fe(II) to seawater can also lead, under specific circumstances, to the formation of amorphous ferrous oxide particles (Bligh and Waite, 2011). Biological surfaces can also contribute with the direct reduction of adsorbed Fe(III) (Maldonado and Price, 2001).

The aim of the present study was to investigate spatial and temporal dynamics of Fe(II) concentrations (measured by chemiluminescence) in the upper 200 m of the water column during the OIF LOHAFEX. The objectives were to present i) the first estimates of dissolved and particle-associated Fe(II) with the intention to shed light on the relevance and chemical form of particulate Fe(II), ii) a description of the temporal evolution of deep DFe(II) and nitrite maxima and iii) repeated measurements of Fe(II) concentrations across OIF bloom boundaries with night and daytime concentrations to evaluate the role of biological processes on iron redox chemistry.

1.1. The LOHAFEX experiment

Ecological and chemical changes were monitored during the austral summer of 2009 following the release of 2 tons of Fe(II) (as $Fe(SO_4)\cdot H_2O$) in a 300 km^2 circular patch in the closed core of a stable cyclonic eddy (R/V *Polarstern*). The eddy was located at 48°S 15°W south of the Antarctic Polar Front, in the Atlantic sector of the Southern Ocean (Fig. 1a). A detailed description of the evolution of the location and extension of the fertilized patch, vertical carbon fluxes, evolution of the microbial and phytoplanktonic communities and changes in iron concentration and organic speciation, can be found in Ebersbach et al. (2014), Laglera et al. (2017), Laglera et al. (2020), Martin et al. (2013), Mazzocchi et al. (2009), Schulz et al. (2018), Smetacek and Naqvi (2010) and Thiele et al. (2012). We found in the mixed layer (ML) of the selected eddy moderate Chl *a* concentrations (0.4–0.5 mg Chl *a* m^{-3}), low but non-depleted DFe concentrations (~0.2 nM) and depleted silicate concentrations (<1 μM). Since 2 days were required for fertilization and repositioning of the ship at the center of the patch, samples of fertilized waters could not be collected during the initial 48 h. Prior iron deficiency was revealed by the rapid response of the phytoplankton community with an increment of F_V/F_M from ~0.33 to 0.4–0.5 at all stations within the fertilized patch. During the first three weeks of the experiment, the center of the patch underwent only moderate dilution (about 50 % by day 20) (Martin et al., 2013). On day 21, a second fertilization of another 2 tons of Fe(II) was carried out along a longitudinal transect covering the length and width of the patch as it drifted by. During the fifth week, the patch reached the eddy boundaries leading to enhanced shear that led to patch fragmentation and dilution (by about 80 % on day 39 after fertilization).

1.2. Main biochemical features during LOHAFEX

The initial Chl *a* standing stock of 39 mg Chl *a* m^{-2} increased upon fertilization substantially to a maximum of 106 mg Chl *a* m^{-2} on day 16 (Fig. 1b) (Martin et al., 2013). Despite patch fragmentation and horizontal dilution, at the end of the experiment on day 39, Chl *a* standing stocks, were still substantially above those of surrounding waters (never below ~70 mg Chl *a* m^{-2}) (Fig. 1b). The plankton community, dominated by nanoflagellates and featureless coccoid cells, increased its biomass but without significant composition shifts (Schulz et al., 2018; Thiele et al., 2014). Diatoms did not increase because of low silicic acid concentration. The phytoplankton biomass was controlled by the increasing grazing pressure of the large copepod *Calanus simillimus* (Mazzocchi et al., 2009).

Export of sinking material remained low throughout the experiment and was dominated by fecal pellets of large copepods (Martin et al.,

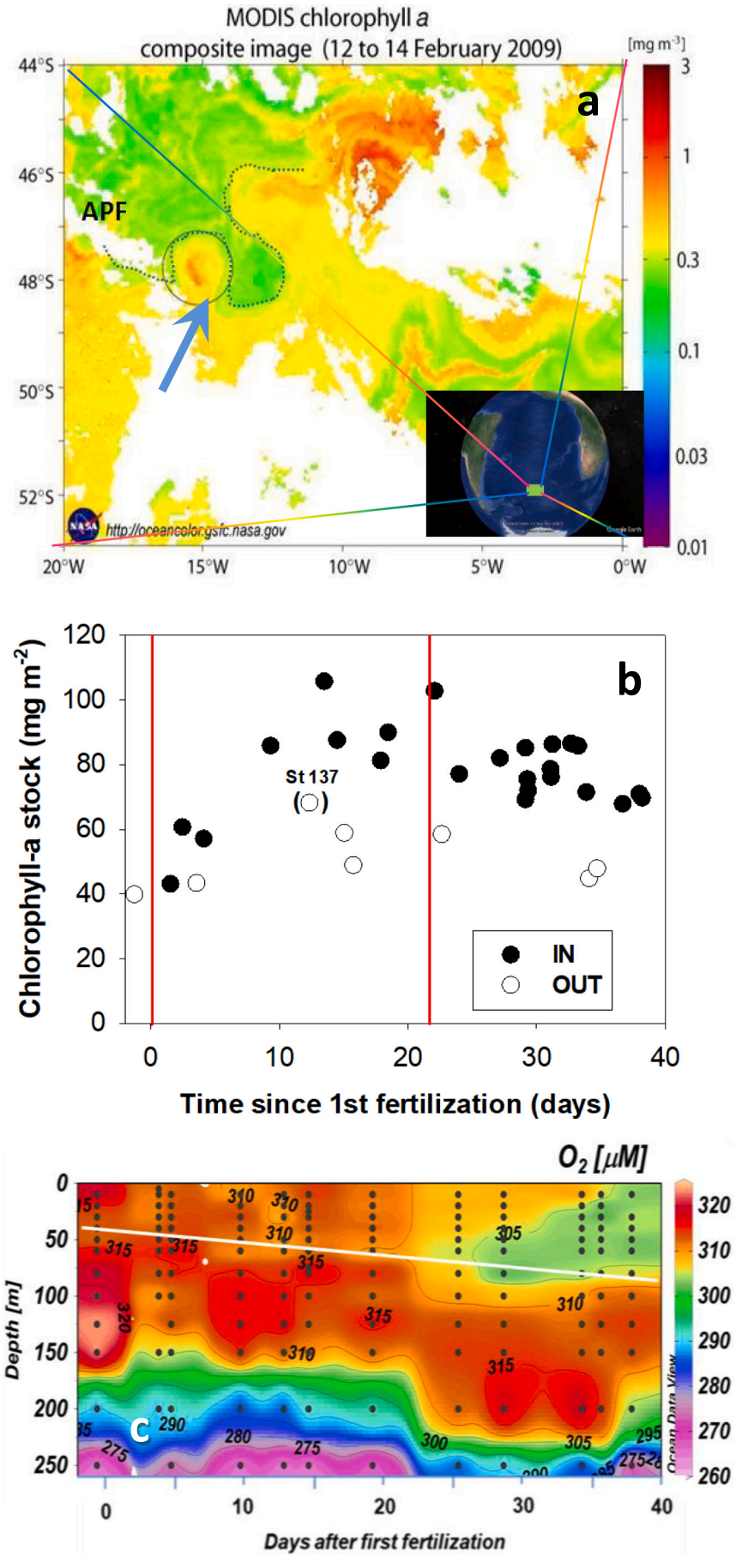

Fig. 1. a: Chlorophyll *a* distribution map for the period 12th to 14th February 2009 from MODIS-Aqua Level 3 data (NASA Goddard Space Flight Center, Ocean Ecology Laboratory, Ocean Biology Processing Group; (2014): MODIS-Aqua Ocean Color Data; NASA Goddard Space Flight Center, Ocean Ecology Laboratory, Ocean Biology Processing Group. https://doi.org/10.5067/AQUA/MODIS_OC.2005.1 (Accessed on 26/06/2009)).The eddy selected to harbor the LOHAFEX experiment is indicated by the blue arrow. The impact of Fe addition is visible from space by the enhanced Chl *a* (red area) within the eddy. The approximate location of the Antarctic Polar Front (APF) is indicated by the dotted line. Note that the overall elevated Chl *a* concentrations South of the APF (including background levels in the eddy) and the intense bloom to the northeast are all induced by natural causes. b: Time course of Chl *a* standing stocks of the fertilized patch (IN stations, full circles) and non-fertilized waters inside the eddy (OUT stations, open circles) during LOHAFEX. c: time course of dissolved oxygen concentrations in the upper 250 m of the water column inside the patch. Mixed layer depths are indicated by the white dotted line. (For interpretation of the references to color in this figure legend, the reader is referred to the web version of this article.)

2013). The efficient remineralization of sinking material within the upper 100–150 m (Ebersbach et al., 2014; Martin et al., 2013) was due to the feeding habits of copepods that include coprophagy (pellet ingestion), coprorhexy (pellet fragmentation) and coprochaly (pellet peeling) (Gonzalez and Smetacek, 1994; Iversen and Poulsen, 2007; Noji et al., 1991).

Chl *a* analysis (Fig. 2a) and satellite pictures (Fig. 1a) confirmed some biomass accumulation during the third week in non-fertilized waters of the selected eddy (maximum at 59 mg Chl *a* m^{-2} on day 15) (Laglera et al., 2017). Many biological and chemical variables did not show significant gradients across the patch boundaries over the duration of the experiment including, remarkably the composition of the phytoplankton community, the zooplankton community, fecal pellet concentrations and vertical export (Martin et al., 2013; Schulz et al., 2018).

1.3. LOHAFEX experiment stages

To simplify the description of the evolution of biological and chemical parameters during LOHAFEX we divided the experiment into three stages. 1) The *growth* stage (days 0–10), defined by a steady increase of Chl *a* concentrations and net community production (NCP), and consumption of nitrate and phosphate. 2) The *grazing* stage (days 10 to 24), defined by stable Chl *a* concentrations and NCP values as a result of the increased grazing pressure. 3) The *dilution* stage (days 25 to 37), characterized by substantial patch dilution, a moderate decrease in Chl *a* concentrations, a decrease in NCP back to zero, stable nutrient concentrations, and a relaxation of the grazing pressure.

1.4. Iron cycling and organic speciation during LOHAFEX

A detailed account of the evolution of dissolved and particulate concentrations of total iron and the organic speciation of iron in the upper 200 m during LOHAFEX have been published before (Laglera et al., 2017; Laglera et al., 2020). Briefly, DFe standing stocks measured in the upper 80 m before and 48 h after the initial fertilization remained approximately constant at ~20 μmol Fe m^{-2} despite an addition equivalent to 120 μmol Fe(II) m^{-2} (or 2 nM over the upper 100 m). Only after day 14, one week before the second fertilization, DFe standing stocks increased two- to three-fold to 40–70 μmol Fe m^{-2}. This increment was surprisingly similar in non-fertilized waters, ruling out horizontal dilution. In the absence of vertical and horizontal gradients, this is indicative of particulate to dissolved fluxes.

The second iron fertilization on day 21, also equivalent to 2 nM over the upper 100 m, had no significant effect on the DFe standing stock three days later confirming again fast oxidation and transfer to the particulate phase. After the second fertilization and until the end of the experiment, fecal pellets released by copepods contained ~5-fold higher iron if captured in fertilized waters, constituting 1/3 of the total iron budget, indicative of a substantial injection of iron into the trophic chain (Laglera et al., 2017).

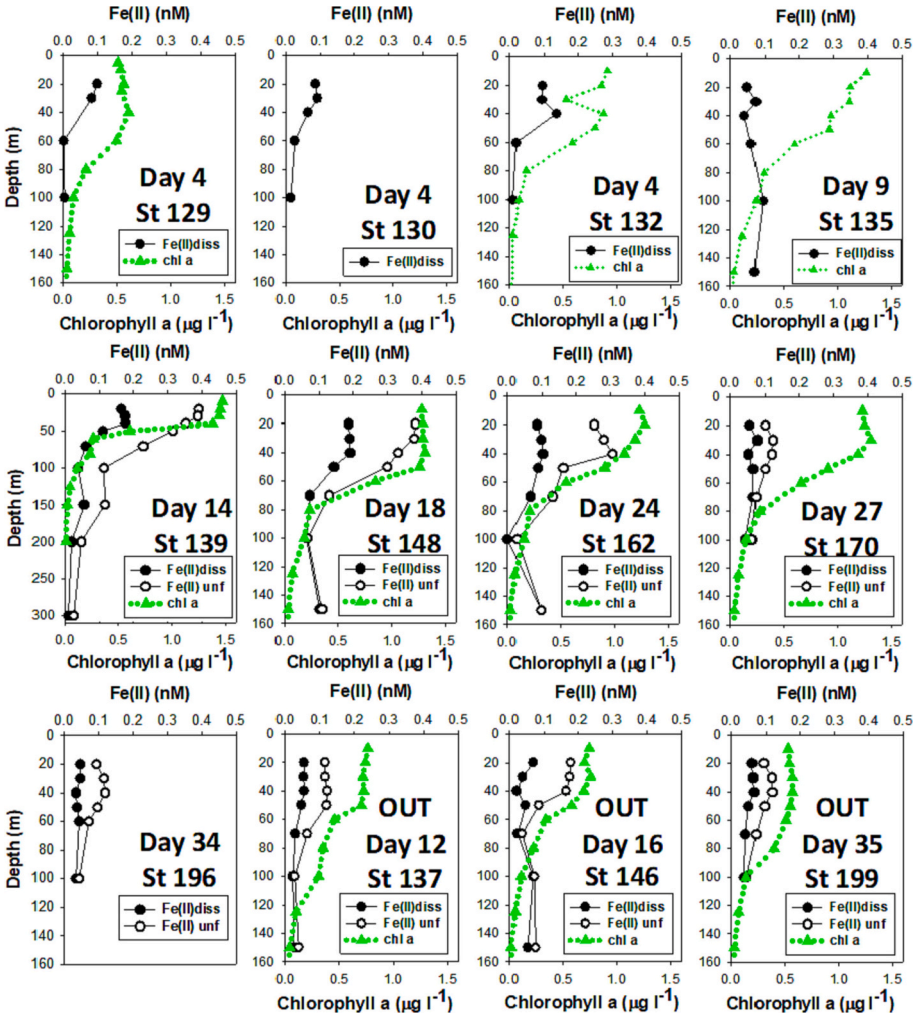

Fig. 2. Vertical distribution of the concentration of chlorophyll, dissolved Fe(II) and total Fe(II) (TFe(II) from unfiltered samples) measured in the upper water column during the LOHAFEX experiment. Note the different depth scale used for Station 139 on day 14.

Dissolved iron ligands (L) were always in great excess compared to DFe concentrations. It is important to remark that L concentrations are always determined after the oxidation of any Fe(II) present in the original sample and do not provide information about the possible presence of specific Fe(II) ligands. Ligand standing stocks in the upper 80 m increased during the first week from 70 to 200–250 μmol m^{-2} and remained at or above 150 μmol ligand m^{-2}. Again, a parallel increase of ligand standing stocks in non-fertilized waters ruled out horizontal dilution. The increase was mostly due to the release and accumulation of an iron ligand class characterized by much higher affinity for iron (L_1) than those dominating iron speciation at the beginning of the experiment (L_2 where $L = L_1 + L_2$) with stability constants $K'_{FeL1} \gg K'_{FeL2}$. Higher-affinity ligands were also found in non-fertilized waters during the second half of the experiment. The decrease in ligand concentrations during the *dilution* stage was caused mostly by the disappearance of L_1 from the upper 40 m of the water column. The temporal dynamic for L_1 points to an intracellular molecule, possibly a pigment, released to the dissolved phase via cell lysis (from a combination of cell death, microbial activity and copepod sloppy feeding). As the grazing pressure relaxed during the *dilution* stage, L_1 release decreased and photodegradation removed L_1 from the upper 40 m of the water column. Below the ML, both DFe and ligands showed substantial increases with time, indicative of remineralization of particulate iron. Lower fecal pellet concentrations below 100 m throughout the experiment, indicated fast epipelagic recycling and explained the late increment of DFe standing stocks and the resilience of the LOHAFEX bloom (Laglera et al., 2017).

Laglera and collaborators proposed that trophic processes were the main cause of the referred dynamics in iron and ligand concentrations. Phagotrophy of iron-rich colloids, typical of flagellates, and posterior copepod grazing on iron-enriched particles (adsorption) and cells (uptake) could explain the fast enrichment in iron of copepod fecal pellets restricted to fertilized waters. Copepod sloppy feeding (the portion of food lost during prey grinding that can amount to ~50 % in C) (Møller et al., 2003) during coprophagy would have promoted the transfer of particulate iron and ligands back into the dissolved pool.

2. Materials and methods

2.1. Seawater sampling

Seawater samples were collected from day 2 of the experiment until day 34 in the so-called "hot spot" (IN stations) of the fertilized patch (Table 1). Additional samples were collected outside the fertilized waters (OUT stations) to discriminate between the effects of fertilization and general processes affecting the eddy. Trace element clean sampling methodology during LOHAFEX has been described in detail elsewhere (Laglera et al., 2017). Briefly, water column samples were collected (usually in the upper 200 m) in Teflon-coated 5 L Niskin bottles mounted in an epoxy-coated aluminum frame (all from General Oceanics). Before subsampling, Niskin bottles were transferred into a plastic box in a cold room to prevent warming. Until day 14, we followed conventional protocols and all samples were filtered immediately prior to analysis for DFe(II). Thereafter, in response to the observed homogeneity of DFe concentrations in the upper 200 m during the *growth* stage, unfiltered samples were also collected and analyzed for total labile Fe(II) (TLFe (II)). Subsampling and immediate analysis was carried out in order of increasing depth.

Table 1
Summary of LOHAFEX stations sampled and analyzed by chemiluminescence. DFe(II): dissolved Fe(II) concentration (<0.2 μm); PFe(II): particulate Fe(II) concentration (>0.2 μm). Prefert.: natural pre-fertilization conditions.

Station	Days after 1st fertiliz.	Days after 2nd fertiliz.	# of depths sampled for DFe(II)/PFe(II)	Location	Radiation (W m^{-2})
114	−1	–	0/0	Prefert.	
121	2	–	2/0	IN	359
126	3	–	1/0	IN	544
129	4.0	–	4/0	IN	170
130	4.5	–	5/0	IN	330
132	4.9	–	5/0	IN	0
135	9	–	6/0	IN	107
137	12	–	7/7	OUT	416
139	14	–	9/9	IN	0
146	16	–	7/7	OUT	
148	18	–	7/7	IN	5
162	24	3	7/7	IN	250
170	27	6	6/6	IN	0
196	34	13	6/6	IN	590
199	35	14	6/6	OUT	2

After collection of the unfiltered samples, a polycarbonate acid-clean capsule filter (0.2 μm, Sartobran 300) was connected to the collection line and flushed with approximately three times its dead volume. Subsequently, samples for the analysis of DFe(II) were taken (approximately 1–2 min after collection of the TLFe(II) sample). Particulate Fe(II) concentrations (PFe(II)) were estimated by subtracting DFe(II) from TLFe (II). Two graduated 250 mL Teflon containers were used to collect subsamples. During subsampling, the containers were rinsed thoroughly with the Niskin outflow (filtered or unfiltered) for wall conditioning before being filled and capped. All containers were rapidly transferred to the lab and kept in ice during analysis to prevent sample warming and Fe (II) oxidation. Typically, DFe(II) or TLFe(II) analyses were completed within 2 min after subsample collection. Sampling containers were stored between stations with ultrapure water to avoid activation by acidification of the container walls.

2.2. Dissolved iron and iron ligands analyses

DFe concentrations, iron ligand concentrations and the analytical protocols used for their determination, have been published before (Laglera et al., 2017; Laglera et al., 2020). Briefly, DFe concentrations were partially measured onboard by voltammetry as in (Laglera et al., 2013) and partly back in the laboratory using Inductively Coupled Plasma-Mass Spectroscopy (ICP-MS) following (Tovar-Sánchez, 2012). Results from a subset of samples analyzed using both methods were in robust agreement (Laglera et al., 2017). Iron ligand concentrations were obtained after equilibration with the competing iron ligand 2,3-dihydroxynaphtalene using adsorptive cathodic stripping voltammetry in the presence of bromate (Laglera et al., 2011; van den Berg, 2006). This analytical method allows the analysis of ligands of biological origin without contributions from most of the humic substances of terrigeneous origin due to their electroactivity.

2.3. Iron(II) reagents and analysis

Ultrapure water for cleaning and reagent preparation was generated on board by means of a Milli-Ro reverse osmosis and a Milli-Q deionizer system from Millipore. Stock solutions 4 mM Fe(II) were prepared weekly onboard by dilution in ultrapure water of pre-weighted ferrous ammonium sulfate (AnalaR, BDH) spiked with HCl (0.2 M final concentration) of the maximum commercially available purity (Merck) to prevent oxidation. Fe(II) standards (20 mL at 10^{-5} M further diluted to 5×10^{-8} M) were prepared daily by dilution of the stock solution with ultrapure water and acidified with HCl to a pH of 1.8. Luminol (Sigma) and K_2CO_3 (Merck) mixed solutions (0.5 mM and 0.1 M, respectively) were prepared onboard after dissolution of pre-weighted reagents in 1 M ammonia buffer (NH_3/NH_4Cl). The pH of this solution was adjusted with HCl and/or NH_3 at 10.5 (NBS) and allowed to rest overnight at least before first use.

The analytical flow injection system was a FeLume(II) (Waterville Analytical) equipped with a photomultiplier (Hamamatsu) to collect the chemiluminescence signal emitted after the mix of the sample with a luminol solution. All tubes were solid black to minimize ambient light

contamination and prevent photochemical reactions inside. To minimize any warming or oxidation of the sample, the usual configuration of the FeLume(II) was modified eliminating the sample loop (Hopkinson and Barbeau, 2007; Laglera and van den Berg, 2007; Rose and Waite, 2001; Shaked, 2008) and continuously pumping samples through the carrier line in the reaction chamber. This setting reduced the subsampling-to-analysis period to approximately 90 s. With this configuration, the output is in the form of a continuous line (Fig. S1). Following standard procedures, the zero Fe(II) concentration was assigned to the signal registered while flushing 0.2 μm filtered seawater collected at 150 m deep and aged at least 2 days in the dark (aged seawater, ASW). We assume that no residual Fe(II) remained stabilized for days in ASW, if that was the case caused by Fe(II) binding, all Fe(II) concentrations could have been slightly underestimated. Aging was at some extent effective as it is proved by the DFe(II) concentrations over the limit of detection found in freshly collected 150 m deep samples (Fig. 2 and Table S1). On the other hand, our setting avoids differences in sensitivity between the carrier and sample solutions.

The sampling and analysis of a whole cast was typically completed in approximately 1 h. ASW was measured before the first sample and several times during the cast analysis to ensure the stability of the baseline. Typically, ASW counts showed 5 % variability (standard deviation on day 9, n = 7), equivalent to a Fe(II) concentration below the limit of detection and without any consistent trend.

Chemiluminescence readings were converted to Fe(II) concentrations after internal calibration by addition of at least 3 Fe(II) spikes close to a concentration of 0.1 nM (actual concentration dependent on the sample volume left in the graduated container). At each station, we calibrated ASW which result we used to calculate concentrations (Fig. S2). For every cast, we also calibrated the deepest filtered and unfiltered samples (Fig. S1 for station 146), and in some cases 20 m deep filtered and unfiltered samples, in order to check for matrix effects that were eventually discarded. During the initial steps of the calibration, the chemiluminescence signal was stable, however, at high Fe(II) concentrations (>0.6 nM) following several additions of the Fe(II) standard, a decrease of the chemiluminescence signal following Fe(II) spikes occurred (Fig. S3). We used this as an indicator to stop the internal calibration. Only the signal that showed stability were computed to find the calibration curve. The implication of finding oxidation rates that depended on the Fe(II) concentration are discussed in Section 3.1. The limit of detection for our experimental setting was determined as three times the standard deviation of the signal noise (baseline data spread) and was typically 0.012 nM Fe(II). The use of corrections for the oxidation of Fe(II) concentrations is considered in Section 3.1.

Chemiluminescence calibration curves showed the typical exponential increase (Fig. S2) and were fitted accordingly using a power law equation with the signal registered in ASW as the value for [Fe(II)] = 0. As expected for curved calibrations, internal calibrations of samples with different initial Fe(II) concentrations showed different apparent slopes and did not overlap. After subtracting the values for ASW from each run, the only calibration where zero readings correspond to [Fe(II)] = 0, all calibrations converged close to a unique curve (details and discussion in Section 3.1).

At the time of the cruise we could not be aware of more recent studies that recommended the addition of chelating agents to avoid interferences from Co(II) and V(IV) on luminol chemistry (Ussher et al., 2009). However, we are confident that these trace elements did not interfere with our determinations. Dissolved and particulate Co and V concentrations were determined in LOHAFEX samples by ICP-MS. Dissolved Co and V concentrations in the samples analyzed were low in the ranges of 9.9 to 34 pM and 9.4 to 25 nM, respectively. Importantly, the variability of the concentrations was temporal but never spatial with profiles without vertical gradients in the upper 200 m. Lack of spatial and temporal oxygen gradients indicate that possibly there were no changes of Co and V redox chemistry (V(IV) generation). In deep filtered samples, we obtained in many cases chemiluminescence signals that differed of the ASW signal by less than the detection limit (in red in Table 1). In the absence of vertical gradients, the contributions of dissolved Co(II) and V(IV) to the chemiluminescence signal were subtracted after using ASW readings for baseline correction.

Superoxide is produced during the analysis as a byproduct of the oxidation of Fe(II) and participates in the oxidation of luminol. We cannot discard the fact that due to the fast and direct injection of sample in the detector, natural superoxide could have influenced the chemistry of luminol to some extent. We assume that this effect was small. In a previous work using the same configuration, seawater previously purged with N_2 (in order to reduce oxygen, the precursor of superoxide) did not show variations in the photoformation of Fe(II) or its later reduction (Laglera and van den Berg, 2007).

2.4. Surface Fe(II) from the underway water supply

The peristaltic pump attached to the ship's all Teflon (except for a safety stainless steel closure valve) tubing system allowed for continuous sampling of seawater at a depth of approximately 11 m below the waterline. This system was used, among others, to provide continuous F_V/F_M measurements and samples for Chl *a* analysis. At eight occasions during transects across the patch, we connected the peristaltic pump of our Felume(II) system directly to the tube carrying the underway seawater in order to measure TLFe(II) concentrations across the patch boundaries. In this case, the time between collection and analysis was reduced to approximately 1 min. Values presented here are the result of averaging 400 chemiluminescent counts (discarding the occasional outliers caused by an air bubble intrusion in the system). The chemiluminescence signal was calibrated with ASW as referred in Section 2.3.

2.5. Fe(II) oxidation kinetics in simulated fertilization conditions

We observed that Fe(II) oxidation kinetics, when present, were dependent on the added concentration. Therefore, the study of the fate of the Fe(II) added during fertilization require the simulation of natural conditions. We added ~2.4 nM Fe(II) (1.25 mL of the 10^{-5} M standard), the Fe(II) concentration used during the fertilization, considering the ML depth, to four 5 L Niskin. The concentration of Fe(II) was monitored until it reached a constant value. For the analysis of unfiltered samples, Niskin bottles were kept cold and airtight until analysis about 2 h after collection. For the analysis of filtered seawater, each full 5 L Niskin was connected to one empty Niskin bottle by their sampling ports with two Masterflex tubes connected by a 0.2 μm pore size filter cartridge. The 5 L seawater was rapidly filtered and transferred (under 1 min) to the empty bottle by applying pressure using nitrogen to the gas port of the full Niskin bottle. A schematic description of the procedure can be found in Fig. S4.

Before starting the analysis, the gas port of the Niskin bottle was connected to a balloon filled with N_2 to prevent the formation of an oxidative headspace. The experiment sequence started by analysis of ASW to obtain the zero Fe(II) baseline. Next, the Niskin bottle was plugged to the Felume(II) and rapidly spiked with the Fe(II) standard solution after opening one end of the Niskin bottle for ~2 s. The Niskin bottle was immediately turned upside down and back twice to homogenize its content. Thereafter, measurements were taken while the Niskin bottle remained still and covered in ice. After Fe(II) oxidation was complete and a steady signal was reached, ASW was analyzed again to check for the stability of the system, calibrated and signals converted to Fe(II) concentrations.

2.6. Other analyses

Chl *a*, O_2, F_V/F_M, nitrite and ammonium concentrations were measured according to standard procedures in oceanography (Smetacek and Naqvi, 2010). Fast Repetition Rate Fluorometer data collected after sunrise was discarded due to the artifacts caused by daylight (Murchie

and Lawson, 2013). Solar radiation was reported as the short-wave downward (GLOBAL) radiation recorded by the onboard pyranometer (Kipp&Zonen CM11). Solar radiation during the cruise ranged from 0 at night to a maximum of 1250 W m^{-2}.

3. Results and discussion

3.1. Fe(II) analysis and Fe(II) oxidation rates

The kinetics of Fe(II) oxidation in seawater have been studied at different pH and temperatures from various locations (Croot et al., 2005; Hopwood et al., 2020; Shaked, 2008). In some instances, these kinetics have been used to correct for possible Fe(II) losses by oxidation during sampling and flow analysis (Kondo and Moffett, 2013; Shaked, 2008), although its use is not generalized. Here, we decided against this correction based on: i) the low temperature of seawater (<6 °C), ii) the patent stability of the chemiluminescence signals of all unfiltered and filtered samples in the range of concentrations we found in our samples (~0–0.39 nM), iii) the stability of the signal after DFe(II) additions during calibrations; this stability was only lost when, after successive ~0.1 nM additions, Fe(II) concentrations exceeded ~0.6 nM (Fig. S3) and iv) the similarity between TLFe(II) concentrations obtained in samples collected with Niskin bottles closed at 20 m deep and with the underway water supply.

At the low temperatures in the study area, redox reactions are slowed down substantially. DFe(II) half-lives in Southern Ocean seawater were found to be approximately 1.5 h (Croot and Laan, 2002), more than the time required to complete our cast, subsample collection and analysis (about 1 h). During analysis of underway samples, the time lapse of 10+ minutes from the in situ closure of the Niskin bottle to analysis was reduced to <1 min. The similarity between TLFe(II) concentrations from casts and underway measurements indicates that TLFe(II) concentrations were stable or that oxidation kinetics was completed in less than a minute (see below for details).

Some previous field works have corrected Fe(II) concentrations using oxidation kinetics, sometimes correcting matrix changes resulting from shifting oxidation kinetics as a function of the sampling depth. These corrections, however, are based in oxidation rates that are not a function of the Fe(II) concentration. During calibrations, we found that in all cases oxidation kinetics were negligible at low DFe(II) concentrations (up to approximately 0.6 nM or 1400–1600 counts) and increased progressively at higher Fe(II) concentration in both filtered and unfiltered samples (Fig. S3). The concentration of 0.6 nM is about 0.2 nM higher than the most concentrated sample we found during the experiment. Maximum oxidation kinetics after Fe(II) spikes at nanomolar range concentrations are discussed in Section 3.5. Experiments back in the lab with UV-digested seawater kept for equilibration at least overnight were not conclusive since the signal was difficult to stabilize to obtain a baseline. Possibly, this was associated to the formation during the digestion step of reactive oxygen species interfering with either Fe(II) or luminol chemistries.

Oxidation kinetics dependent on the Fe(II) concentration spiked do not concur with the independence of Fe(II) oxidation rates found in deep North Atlantic waters (3100 m) measured after spiking samples with Fe (II) concentrations in the 0.48 to 4.83 nM Fe(II) range (Santana-González et al., 2018). It is important to remark that our spikes that gave stable signals never went over ~0.4 nM Fe(II) and our experiments were restricted to waters in the upper 200 m where biological derived organics are likely at higher concentrations. From a conceptual framework, we have to consider that different components of the natural organic matter pool occasionally accelerate or usually slow down Fe(II) oxidation rates (González et al., 2014; González et al., 2012; Pérez-Almeida et al., 2022; Rose and Waite, 2002; Santana-González et al., 2019; Ussher et al., 2005). Fe(II) bound to stabilizing ligands must oxidize at slower rates than free Fe(II). In the presence of these organics, the Fe(II) oxidation rate must be a function of the ratio of the concentration of interfering organics and the initial Fe(II) concentration (Hopwood et al., 2017). Therefore, specific Fe(II) organic ligands at low concentrations, could have become saturated as we incremented Fe(II) concentrations during the titration. Fe(II) oxidation kinetics also usually show strong horizontal, vertical and temporal gradients (Santana-González et al., 2018; Sarthou et al., 2011). Therefore, simple pseudo-first order corrections could introduce as much bias as purportedly preventing it.

3.2. Dissolved Fe(II) concentrations during LOHAFEX

All Fe(II) data (dissolved and particulate) can be found in Table S1 and vertical profiles are presented in Fig. 2. Throughout the experiment, typical DFe(II) profiles in fertilized ML waters showed higher concentrations in the upper 50 m, decreasing steeply down to 70 m and remaining low in deeper waters. At OUT stations, DFe(II) accumulation in the upper 50 m was minor and concentrations remained low (<0.07 nM) (Fig. 2).

The temporal evolution of DFe(II) concentrations in fertilized waters down to 150 m is shown in Fig. 3b. DFe(II) concentrations in the ML were consistently low at 0.03–0.07 nM at the beginning of our sampling (days 2 to 4) and increased substantially during the *growth* stage peaking during the *grazing* stage at ~0.19 nM (an up to ~6-fold increment). Accumulation of DFe(II) in the ML days after an OIF was also observed during SOIREE and hypothesized to be caused by extracellular enzymatic reduction (Croot et al., 2001). Surprisingly, 4 days after the second fertilization on day 21, DFe(II) concentrations in the ML were low and decreased further to ~0.07 nM on day 34 reaching values similar to those recorded at the beginning of the experiment and at OUT stations.

Below the ML, although we could not get the same time and spatial resolution, the DFe(II) evolution seemed very patchy. DFe(II) concentrations at 80–100 m were low, but at the depth range of 100–150 m a deep maximum at ~0.1 nM was easily recognizable.

DFe(II) contributed 0 to 71 % to DFe depending on depth and time with the highest values consistently at 40 m deep during the grazing stage (Fig. 3G). No other biological or chemical variable correlated significantly with DFe(II) percentages. High contributions of Fe(II) to DFe standing stocks (24–65 %) have also been found in Subarctic waters and coastal mesocosms deployed at high latitude (Hopwood et al., 2020; Roy et al., 2008).

The absence of high DFe(II) concentrations measured 2 to 4 days after both fertilizations (corresponding each to an addition of 2.4 nM Fe (II) throughout the ML) is in agreement with the low DFe concentrations (below ~0.25 nM) found in the same samples (Fig. 3c) (Laglera et al., 2017). This absence concurs with the hypothesis presented by Laglera and coauthors: the added DFe(II) underwent fast transfer to the particulate fraction in a period shorter than two days (the period required to complete the fertilization and relocate the ship back into the patch "hot spot"). Transfer to the particulate fraction could be the result of biological uptake, adsorption (as PFe(II) or PFe(III)) or aggregation (and subsequent sinking). Given the lack of analysis of unfiltered samples before day 14, the fate of Fe(II) added during the first fertilization remains unclear.

3.3. Interpretation of the chemiluminescence signal of unfiltered samples

During our study, the difference between the chemiluminescence signals of filtered and unfiltered samples was substantial at surface (2 to 3-fold) and decreased reaching the detection limit below 70 m (Fig. 2 and S1). The same concerns about the interpretation of chemiluminescence signals in filtered samples discussed in Section 3.1 apply to unfiltered samples, but extended to possible contributions from particle components.

Many organisms, including some flagellates, diatoms, copepods and bacteria, all of them present at significant concentrations during LOHAFEX, naturally glow (Haddock et al., 2010). Since standard

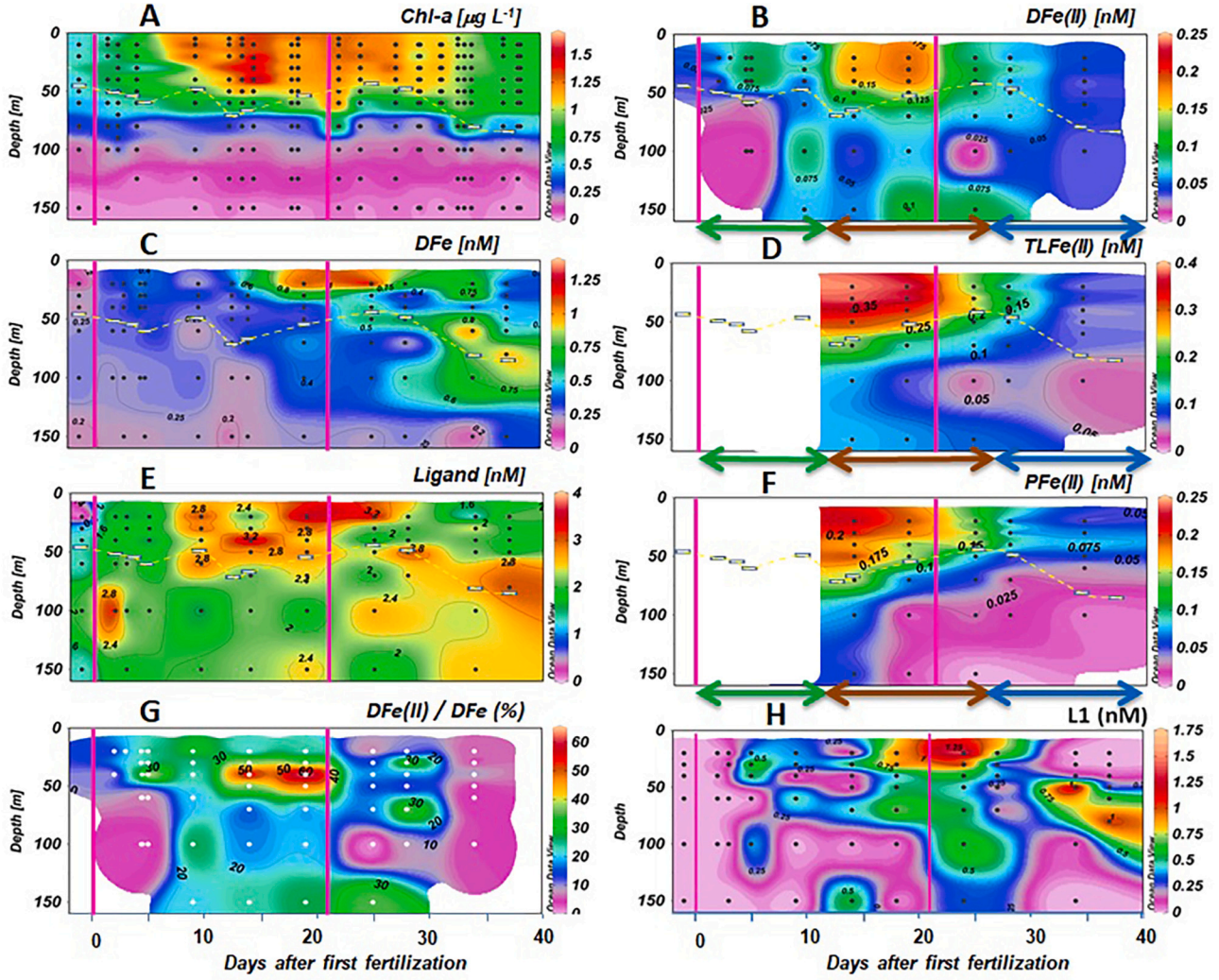

Fig. 3. Time course of (A) chlorophyll-*a*, (B) DFe(II) (<0.2 μm), (C) dissolved iron (<0.2 μm) (Laglera et al., 2017), (D) total iron (TLFe(II)), (E) dissolved iron ligands (Laglera et al., 2020), (F) particulate iron(II) (>0.2 μm) concentrations and (G) the contribution of DFe(II) in % to DFe in the upper 150 m of the water column in fertilized waters during LOHAFEX. (H) is the temporal evolution of strong L1 ligands in fertilized waters (determined using a two ligands –L1 and L2- model) during LOHAFEX. Areas in purple correspond to samples where strong L1 ligands could not be detected (Laglera et al., 2020).The vertical pink lines mark the two fertilization events. The dashed white line marks the depth of the mixed layer in fertilized waters reported before (Martin et al., 2013). The different stages of the experiment are indicated in panels B and D by horizontal double arrows (green: *growth*, brown: *grazing* and blue: *dilution*). (For interpretation of the references to color in this figure legend, the reader is referred to the web version of this article.)

photomultipliers are not specific to the wavelength emitted by the luminol chemistry, natural bioluminescence could have contributed to our analytical signal in unfiltered samples if survived transport through the peristaltic pumps and mixing with reagents. Ocean bioluminescence is ubiquitous and seems related to the composition of the biological community with an important contributions from krill (Melnik et al., 2021) that conveniently was absent throughout LOHAFEX. Southern Ocean bioluminescence profiles show consistent subsurface maxima with similar values at 10 and 70 m (as opposed to our smooth S-shaped PFe(II) profiles) and higher values at night (Melnik et al., 2021), as opposed to our PLFe(II) concentrations which magnitude depended more on the experiment stage than in the irradiance (see Sections 3.4 and 3.8). In order to accelerate the transport of the sample to the detector we selected small diameter tubes (0.8 mm inner diameter) that would prevent the pass of nearly all copepods, which composed nearly all macrozooplankton biomass. Moreover, concentrations of the most abundant copepod, *Oithona similis* (Mazzocchi et al., 2009), were in the order of units per liter and since we only required a few tens of mL per sample, copepod bioluminescence could not represent a significant portion of our stable chemiluminescence signals (Fig. S1). A possible contribution of plankton and bacteria could be supported by the high correlation of PFe(II) and Chl *a* in individual profiles (Fig. 2) and the 2 fold higher concentrations of bacteria found in the ML with respect to 100 m deep (Singh et al., 2015; Thiele et al., 2012). However, the chemiluminescence signal in unfiltered samples decreased substantially during the last stage of the experiment despite the stability of community compositions and standing stocks of both plankton and bacteria. Bioluminescence can also appear as a reaction to induced shear-stress by the pressure produced by high flow during sample pumping into the chemiluminescence detector in the form of an initial pulse, but this contribution in unlikely based in its short life, <10 s (Maldonado and Latz, 2007). Initial tests in the underwater system with different tubes lengths did not show signal variations and again, during the last week of the experiment we got nearly zero signals despite the stability of the bacterial nad planktonic standing stocks.

To test the effect of planktonic cells, ASW was spiked with high concentrations of viable *Phaeocystis* cf. *antarctica*, *Fragilariopsis kerguelensis* and *Pseudonitzschia lineola* cells cultured onboard. Cultures were maintained using EDTA as chelating agent impeding trace element precipitation but also the adsorption of trace elements to particle

surfaces. Since EDTA interferes with the chemiluminescence signal (Bolster et al., 2018), all filters used to accumulate the cells were rinsed several times with ASW before resuspension in ASW. The same experiment was repeated using Chl *a* from the solution used to calibrate Chl *a* fluorescent measurements and large copepod fecal pellets freshly collected (EDTA free in this case) where it is well known that bacteria accumulate on their surface in high numbers. Upon Chl *a*, cell and pellets spikes, the chemiluminescence signal remained undisturbed indicating that in front of the photomultiplier there was no contribution of bioluminescence caused by flow stress, cell lysis nor the bacteria present at the surface of fecal pellets. Moreover, any intracellular and intra-peritrophic fecal pellet membrane Fe(II) did not contribute to the PFe(II) values reported here.

Although hereafter we will consider the contribution of bioluminescence negligible, we are aware that more studies under controlled biological conditions are required and we do not support that our interpretation is applicable to every oceanic biological community.

Interfering chemical species could also contribute to the chemiluminescence signal if adsorbed onto particles. Although the adsorption of superoxide to inorganic surfaces has been confirmed during the study of metal oxide suspensions (Wang et al., 2017), this has not been studied yet in seawater. Since superoxide decay in seawater takes only a few seconds (Heller and Croot, 2010) and we obtained similar chemiluminescence signals using Niskin bottle sampling and continuous underway sampling, we assume that its contribution to our PFe(II) is negligible. Dissolved and particulate Co and V concentrations did not show substantial vertical variations in the upper 200 m during LOHAFEX, since we found negligible PLFe(II) concentrations in deep samples, Co and V could not contribute to the chemiluminescence of surface samples. Interferences from organic substances on the chemiluminescence chemistry of luminol have been hypothesized before and it could be that they were present adsorbed onto particles (Croot and Laan, 2002; Bolster et al., 2018). We claim that such potential interferences were negligible during our analysis based on the similarity of calibrations in filtered and unfiltered samples (Fig. S5), the correlation of PFe(II) with biological variables (Fig. 2) experiments performed after the addition of Fe(II) to filtered and unfiltered samples (see Section 3.5) and the stability of the signal registered in the same water mass over time and space during underwater sampling (see Sections 3.6 and 3.7). We will assume hereafter that the increment of signal in unfiltered samples was due exclusively to Fe(II). However, we want to remark that further experiments with particles surfaces loaded with specific interfering species must be conducted in the future to discard significant interferences especially at low Fe(II) concentrations.

Sensitivity artifacts by the use of calibrations of filtered ASW to determine PFe(II) concentrations were ruled out. This is based on the convergence to a single curve of calibrations of ASW, and filtered and unfiltered samples from different depths from the same run if the initial chemiluminescence signal of sample calibrations were corrected using the ASW calibration to calculate the sample Fe(II) concentration (Fig. S5). We also consider here that the sensitivity of free, complexed and adsorbed Fe(II) were the same. This is based on the nature of the analytical reaction (light is emitted after luminol is excited by the byproducts of the fast oxidation of Fe(II) at the alkaline pH of the luminol solution) that should not be affected by most of the binding groups found in natural waters (Ussher et al., 2005). The interaction of the luminol solution and the binding groups of biological surfaces and/or inorganic aggregates is also not likely to be restricted at the turbulent conditions during the mixing of the two solutions.

3.4. Fe(II) in the particulate phase during LOHAFEX

Our TLFe(II) concentrations showed vertical profiles with the same sharp decrease at 50 to 70 m shown in DFe(II) profiles (Fig. 2) and the same rise and fall in fertilized waters over the duration of the experiment (Fig. 3d). During the *grazing* stage, TLFe(II) in the upper 40 m of the water column peaked (values up to 0.39 nM, about double of the maximum DFe(II) concentration) and decreased during the last stage (values <0.08 nM). TFe(II) concentrations at 150 m showed the same maximum found for DFe(II) (Fig. 3d).

PFe(II) concentrations (from TFe(II)-DFe(II)) (Fig. 3f), gave a time course plot without the patchiness found for DFe(II) (Fig. 3b). PFe(II) also accumulated in the ML, peaking during the *grazing* stage at 0.23 nM and decreasing during the *dilution* stage to values below 0.08 nM. Below the ML, there was no PFe(II) secondary maximum at 150 m (Fig. 3f). At OUT stations, PFe(II) concentrations in the ML reached 0.14 nM on day 16, coincident with a moderate increase of Chl *a* concentrations in the eddy (Fig. 2). For the rest of the experiment, PFe(II) concentrations at OUT stations remained below 0.07 nM in the ML and around the detection limit below the ML. The Pearson correlation coefficient of DFe(II) and PFe(II) was high at $r = 0.720$ ($p < 0.001$, $n = 55$), and further increased slightly to $r = 0.75$ ($p < 0.001$, $n = 40$), despite the reduction of the sample size, for data in the upper 80 m of the water column. These high correlations suggest that the processes controlling DFe(II) and PFe(II) are similar in the ML but different from the processes controlling the accumulation of DFe(II) at 150 m where PFe(II) was absent (Fig. 3b and f).

3.5. Oxidation kinetics in simulated fertilization conditions

Evolution of the Fe(II) added to filtered and unfiltered seawater (collected in fertilized and OUT stations) in the on-board experiments on Fe(II) oxidation kinetics at the same concentration that would have been reached in the ML layer are shown in Fig. 4 and S6. Here, the increment of the signal during the analysis was completely caused by the Fe(II) spike, therefore, analytical artifacts such as sampling-to-analysis delays or interferences from other chemical species such as superoxide or other trace elements can be ruled out. After the spike, Fe(II) concentrations decreased rapidly due to the oxidation of Fe(II) until a steady concentration was reached after roughly 2 h. Fe(II) concentrations returned exactly to the initial values in both filtered samples, while Fe(II) reached a steady state concentration approximately twice the initial value in unfiltered seawater (Table 2, Fig. 4). This is the first experimental evidence of the ability of particle surfaces to stabilize Fe(II). This result also can explain how both fertilizations left no trace in DFe(II) concentrations after 2 days. The lack of fast return to the initial also supports our claim that most of the chemiluminescent signal in unfiltered samples was due to the presence of labile particulate Fe(II). If our signal was a combination of DFe(II) and natural bioluminescence, the signal would have returned to the initial value after the oxidation of DFe(II).

The four experiments gave oxidation rates similar to each other with a Fe(II) half-life in the narrow range of 10 to 15 min (Table 2). The fast kinetics are in agreement with the acceleration of Fe(II) oxidation kinetics at higher Fe(II) concentrations that we observed during calibrations (Fig. S4). In this set of experiments, organic matter that could delay Fe(II) oxidation kinetics was possibly saturated and the oxidation kinetics of the excess (and free) Fe(II) were only dependent on the local concentration of known oxidant species such as O_2 or H_2O_2. Our half-lives are substantially shorter than values previously reported for cold waters (Croot and Laan, 2002) but concur with the lower end of the range of recent results obtained in surface waters of the North Atlantic (Santana-González et al., 2018). It also should be noted that the outcome of the experiments did not depend on whether seawater had been collected in fertilized or non-fertilized waters (Table 2).

Our experiment with several unfiltered 1 L samples spiked with 0.5 nM DFe(II) and kept cold in the dark for days showed that TLFe(II) also decreased back to initial concentrations (0.04–0.08 nM) within 12 h (Fig. S7). In contrast to DFe(II), TLFe(II) concentrations above the detection limit persisted for 3 to 4 days (Fig. S7) showing either the resilience of a fraction of PFe(II) to oxidation or dark formation of Fe(II) by particles. This effect could be even higher since we cannot rule out a small contribution of microbial uptake. This kinetics also explains the

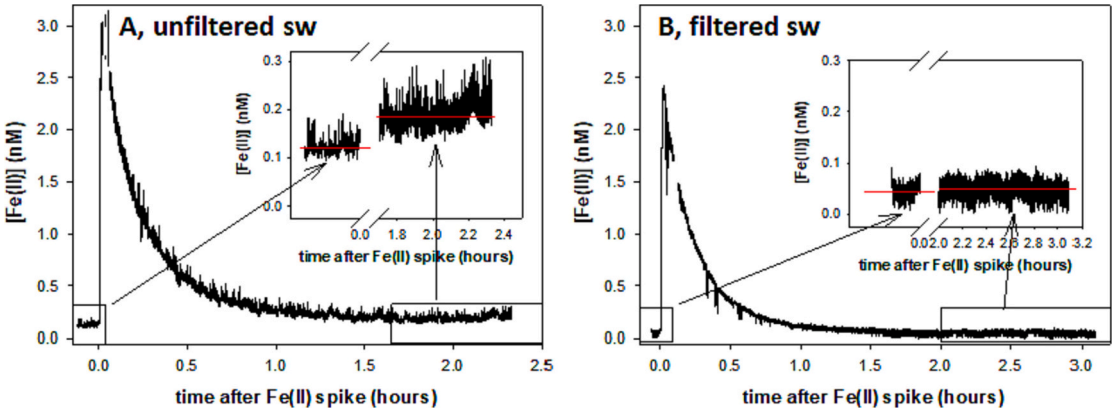

Fig. 4. Evolution of Fe(II) concentrations in two 5 L Niskin bottles filled with unfiltered (A, St. 160, day 23) and filtered (B, St. 162, day 24) seawater before and after the addition of 2.7 and 2.4 nM Fe(II), respectively. The inserted plots show the respective initial and final data in both experiments highlighting the difference between initial and final concentrations exclusive of unfiltered waters (panel a).

Table 2
Fe(II) oxidation kinetic parameters after the addition of approximately 2.5 nM Fe(II) to four 5 L Niskin bottles (2 filtered and 2 unfiltered). The initial 30 min were fitted to a pseudo-first order reaction order and the apparent oxidation kinetics rate constants ($K_{app,ox}$) and Fe(II) half-lives were calculated accordingly. The last 3 columns show the Fe(II) concentrations before spiking (t = 0) and the remaining concentration at the end of the experiment (~2 h later) as well as the percentage of the spike (% addition left) measured at the end of the experiment.

Sample code	Treatment	$K_{app,ox}$ (first 30 min) (h^{-1})	Half life (30 min) (min)	Fe(II) t = 0 (nM)	Fe(II) end (nM)	% addition left
St 160 (OUT)	Unfiltered +2.5 nM Fe(II)	2.86	14.6	0.122 ± 0.006	0.224 ± 0.018	3.8 %
St 183 (IN)	Unfiltered +2.7 nM Fe(II)	3.00	13.9	0.119 ± 0.024	0.240 ± 0.029	4.5 %
St 162 (IN)	Filtered 0.2 μm +2.5 nM Fe(II)	4.03	10.3	0.049 ± 0.014	0.049 ± 0.014	0 %
St 199 (OUT)	Filtered 0.2 μm +2.7 nM Fe(II)	1.98	12.6	0.015 ± 0.016	0.027 ± 0.010	0.4 %

low PFe(II) concentrations measured 2 days after the second fertilization.

3.6. TLFe(II) continuous measurements from the ship underway intake system

The patch location and size were determined from F_V/F_M and Chl *a* gradients measured during longitudinal and transversal crossings using the ship underway intake system. In some transects, TLFe(II) concentrations were simultaneously determined. Filtration for DFe(II) measurements was not carried out during underway sampling due to variations in the biomass load of filters, and as a consequence filtration rates and sensitivity fluctuations caused by variable luminol solution to seawater flow ratios. TLFe(II) distributions are shown in Figs. 5 (night transects) and 6 (transects extending after dawn). It is important to remark that TLFe(II) variations were both spatial and temporal as crossing the patch could take up to a couple hours at full steam.

In all night transects, collected a few days after the second fertilization, F_V/F_M across the patch boundaries increased from ~0.35 to ~0.45 and Chl *a* concentrations approximately doubled from ~0.6 to ~1.3 mg m^{-3} (Fig. 5). TLFe(II) concentrations varied in the ranges of 0.2 to 0.35 nM and 0.1 to 0.25 nM inside and outside the patch, respectively (a 1.5 to 2.5-fold difference) (Fig. 5). This gradient is in agreement with the lower surface TLFe(II) concentrations found at OUT stations (Fig. 2). Variations in TLFe(II) concentrations in night-time measurements (Fig. 5) were strikingly correlated to the variations in Chl *a* and F_V/F_M, pointing to the relevance of biological processes. Pearson correlation coefficients for data shown in Fig. 5 were always higher than 0.82 for TLFe(II) vs F_V/F_M (Table 3). A similar high Fe(II) vs F_V/F_M correlation was found during SOFEX (Croot et al., 2008). The TLFe(II) vs Chl *a* correlations were also high but not all significant due to the lower Chl *a* sampling frequency and therefore smaller datasets that increased the probability statistic p-value ($p > 0.05$ in one case).

The residence time of seawater in the underway system before reaching the chemiluminescent cell was about 1 min, significantly shorter than the time necessary to process the bottle samples taken at stations. TLFe(II) concentration ranges in both types of samples showed strong similarities with values ranging between 0.2 and 0.35 nM in bottle samples (Figs. 2 and 3d) and 0.15 to 0.3 nM in underway samples (Fig. 5), respectively. This indicates that losses due to Fe(II) oxidation were either negligible within the 10 to 15 min needed from bottle closure to process the surface sample or faster than 1 min (a decay rate that would be missed by both methods).

The relationship between underway Fe(II) concentrations and other variables after sunrise presented a more complex scenario (Fig. 6). F_V/F_M ratios were in the same range as found at night when solar radiation was below ~200 W m^{-2}. Above this threshold, F_V/F_M ratios dropped and became unreliable due to daylight quenching. Another source of variability probably comes from the fact that the daytime data covers the three stages of LOHAFEX (from day 6 to 27). Overall, TLFe(II) concentrations were in the same range as in bottle samples or nighttime measurements with the exception of day 6 where TLFe(II) concentrations peaked at 0.56 nM. This concentration is about 50 % higher than the highest concentration obtained from day 14 onwards when TLFe(II) was started to be analyzed in the bottle samples. Given that DFe(II) concentrations in the water column were low (<0.1 nM; Fig. 2), most of the Fe(II) measured on day 6 must have been associated to the PFe(II) pool. TLFe(II) and Chl *a* showed an overall high correlation on day 6 ($r = 0.71$, $p = 0.001$) although a visual inspection reveals that TLFe(II) concentrations barely followed the rise and fall patterns of Chl *a* and F_V/F_M across the patch boundaries. TLFe(II) concentrations on day 6 were better related to solar radiation than to biological variables (Fig. 6). On day 9, TLFe(II) concentrations (0.18–0.3 nM) were substantially lower than the concentrations measured on day 6 with only a moderate increase after sunrise and no correlation to Chl *a* or F_V/F_M (Table 3, Fig. 6). Lower concentrations could be caused by solar radiation remaining below the ~200 W m^{-2} threshold. The situation changed drastically between day 9 and day 18, end of the *grazing* period. On day 18, as long

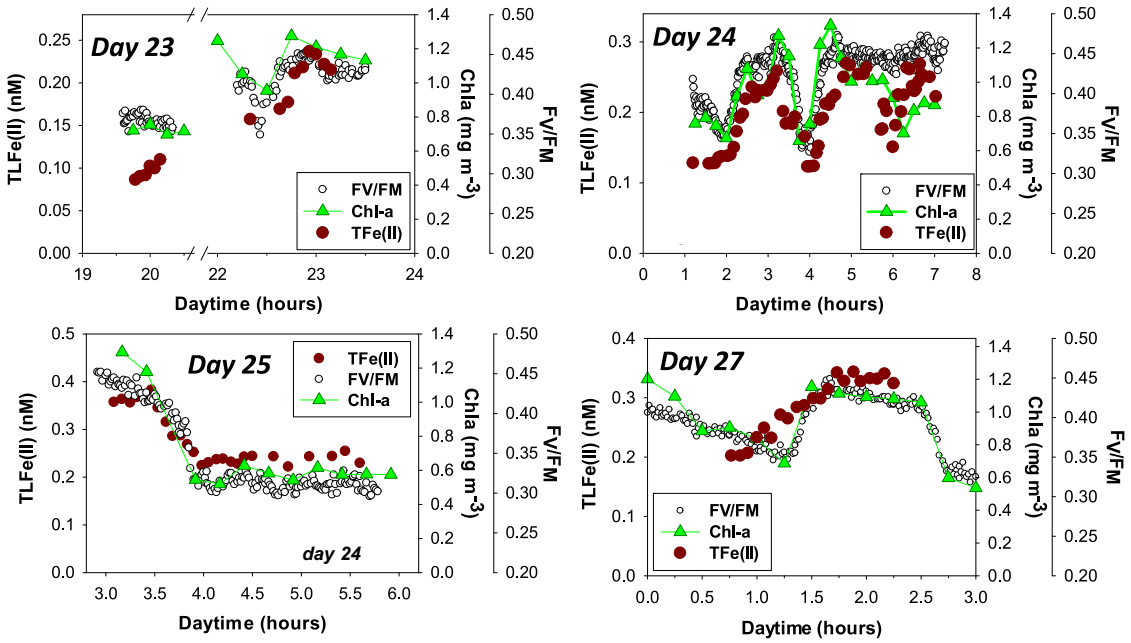

Fig. 5. Photosynthetic quantum efficiency ratios (F_V/F_M), chlorophyll-*a* concentrations and TLFe(II) concentrations in unfiltered samples pumped continuously through the underway ship system while crossing the LOHAFEX bloom at night on four different occasions. F_V/F_M and Chl *a* gradients mark the patch boundaries.

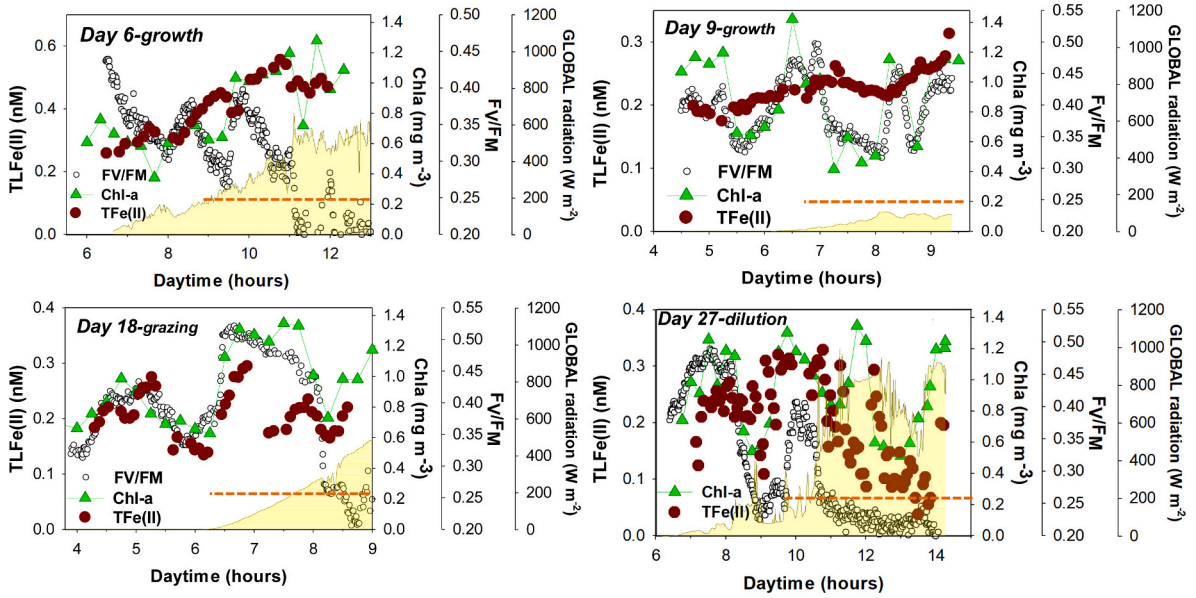

Fig. 6. Photosynthetic quantum efficiency ratios (F_V/F_M), chlorophyll-*a* concentrations, short-wavelength downward (GLOBAL) radiation and TLFe(II) concentrations in unfiltered samples pumped continuously through the underway ship system while crossing the LOHAFEX bloom before and after dawn on four different dates. The maximum value of radiation (Y–axis) is equivalent to the maximum GLOBAL radiation measured at midday during the LOHAFEX cruise.

as the radiation was below the ~200 W m^{-2} threshold, TLFe(II) concentrations (0.12–0.3 nM) followed and were highly correlated with Chl *a* and F_V/F_M in a situation identical to that observed in night transects (day 18 night data in Table 3). At solar radiations above the threshold, daylight TLFe(II) concentrations were similar to dark concentrations (0.17–0.22 nM) but interestingly showed less variability than the other variables across the patch boundaries (loss of correlation, Table 3). On day 27, TLFe(II) concentrations showed a wider range (0.04–0.31 nM) than water column TLFe(II) concentrations around that day (~0.2 nM) (Fig. 3d). Due to a cloudy early morning, solar radiation was near the ~200 W m^{-2} threshold from 8:00 to 10:20 a.m. and all correlations in that early period were very low and not significant ($p > 0.05$). With the substantial increase in solar radiation after 10:20 a.m., TLFe(II) concentrations became patchy and did not follow the highs and lows of Chl *a* concentrations.

Our data indicate that during LOHAFEX there were dark reduction processes in surface waters that were far more effective in fertilized waters and varied substantially during the experiment. During daytime, other processes activated by solar radiation that removed the gradients across patch boundaries, slightly decreased TLFe(II) concentrations. Hereafter, we will try to estimate the weight of known biogeochemical processes in the iron redox speciation during LOHAFEX.

Table 3
Pearson correlation coefficients (r), significance (p) and sample size (n) for the data shown in Fig. 5. The p-values larger than 0.01 are in bold. ns: not significant due to low r and high p.

	TLFe(II) vs Chl-a	TLFe(II) vs F_V/F_M	Chl-*a* vs FV/FM
Day 23	r = 0.934	r = 0.937	r = 0.968
	(p < 0.001) n = 10	(p < 0.001) n = 15	(p < 0.001) n = 15
Day 24	r = 0.525	r = 0.834	r = 0.636
	(p = 0.006) n = 26	(p < 0.001) n = 59	(p < 0.001) n = 26
Day 25	r = 0.969	r = 0.942	r = 0.985
	(p < 0.001) n = 12	(p < 0.001) n = 34	(p < 0.001) n = 12
Day 28	r = 0.672	r = 0.823	r = 0.956
	(**p = 0.098**) n = 7	(p < 0.001) n = 25	(p < 0.001) n = 7
Day 6	r = 0.708	ns	ns
	(p = 0.001) n = 18		
Day 9	r = 0.708	r = 0.224	r = 0.800
	(**p = 0.547**) n = 19	(**p = 0.071**) n = 66	(p < 0.001) n = 19
Day 18 (all)	r = 0.416	r = 0.567	r = 0.628
	(**p = 0.097**) n = 17	(p < 0.001) n = 48	(p < 0.001) n = 19
Day 18 (night)	r = 0.707	r = 0.784	r = 0.916
	(**p = 0.022**) n = 10	(p < 0.001) n = 30	(p < 0.001) n = 12

3.7. On the chemical nature of dissolved and particulate Fe(II) species

The return to the initial concentration during our oxidation experiments (Fig. 4) suggests that DFe(II) was at or close to its maximum possible concentration. However, DFe(II) concentrations increased 6-fold to later decline in the same proportion while the chemiluminescent signals always showed stability throughout the experiment. Such variability, despite sampling under different solar radiation conditions, and the fast and complete oxidation (few hours) of Fe(II) from the fertilization, points to a control of iron redox speciation by local biological processes. We hypothesize that our samples contained dissolved Fe(II) specific ligands, close to saturation under our physicochemical conditions. Thee ligands were similar to those proposed in previous studies from other oceanic areas (Roy et al., 2008; Santana-González et al., 2019), model compounds (González et al., 2019) or algal cultures (González et al., 2014) that delay substantially Fe(II) oxidation, or may even promote Fe(III) reduction (Arreguin et al., 2021; Pérez-Almeida et al., 2022). This implies that substantial concentrations of these ligands were released by biota and accumulated in the ML during the two first stages of the experiment and disappeared during the last stage of the experiment. These stabilizing ligands (at concentrations of tens to hundreds of pM) would mark the solubility limit of DFe(II). This scheme is in agreement with the higher oxidation rates measured at higher Fe(II) concentrations during internal calibrations. In contrast, our kinetics experiments with unfiltered samples indicate that particle surfaces were not initially saturated with surface binding groups available to stabilize a fraction of the DFe(II) supplied.

Comparing PFe(II) concentrations to particulate iron, PFe(II+III) concentrations determined by standard protocols, is not straightforward. PFe(II+III) concentrations are obtained after total or partial particle dissolution by acidification and/or microwave digestion altering the redox speciation. Since chemiluminescence is fast and our methodology was determined to not produce significant particle disaggregation, we hypothesize that PFe(II) measured with standard chemiluminescence protocols comprises only adsorbed Fe(II) onto particles.

The Fe(II+III) pool in phytoplankton cells is distributed between internal and surface adsorbed fractions. Extracellular iron (mainly Fe oxides) accounted for up to 16–86 % of the total cellular concentration in samples from the Southern Ocean (Tovar-Sanchez et al., 2003). Chemiluminescence signals from the analysis of unfiltered samples collected at high Chl *a* concentrations in the ML showed not just higher values but also more scattering than any filtered and deep unfiltered samples (Fig. S8). High concentrations of PFe(II+III) were found at days 14 and 18 (up to 6 nM) at 50 to 100 m depth, probably inorganic aggregates lasting from the initial fertilization (Laglera et al., 2017). Figs. 2 and 3f show that no PFe(II) anomalies could be detected in those samples which we interpret as the absence of significant concentrations of adsorbed Fe(II) on iron aggregates. We therefore conclude that PFe(II) concentrations correspond mainly to Fe(II) adsorbed onto organic surfaces although empirical confirmation would have required experiments in conditions not available onboard.

3.8. Abiotic processes: oxygen and solar radiation effects on Fe(II) concentrations during LOHAFEX

Globally, hypoxia, including expanding oxygen minimum zones, is the main cause of chemical and microbial DFe(II) formation and stabilization in the ocean (Kondo and Moffett, 2013; Lohan and Bruland, 2008; Schlosser et al., 2018). However, during LOHAFEX, O_2 concentrations in the ML did not show any decrease until the *dilution* stage which was coupled to a decrease of surface DFe(II) and PFe(II) concentrations (Fig. 1c). Below the ML, O_2 concentrations between 100 and 150 m remained high and even increased. Hence, changes in O_2 could not have contributed to formation of the deep DFe(II) maximum (Fig. 1c).

Diurnal cycles of the Fe redox speciation in the ML have been reported in numerous studies (Bowie et al., 2002; Rijkenberg et al., 2005; Waite et al., 1995) including daytime transects in previous OIF experiments (Croot et al., 2001; Roy et al., 2008). These diurnal variations have been interpreted as the result of the stabilization of freshly photoproduced Fe(II) by uncharacterized Fe(II) specific ligands (Hopwood et al., 2020). During LOHAFEX, however, diurnal variations of Fe(II) concentrations cannot be explained by photoproduction and stabilization of Fe(II) by uncharacterized Fe(II) specific ligands for at least three reasons. Firstly, daytime measurements did not show an increase in TLFe(II) concentrations (Fig. 6). Secondly, no relationship between DFe(II) as well as PFe(II) standing stocks in the upper 60 m of the water column and the GLOBAL radiation measured during the clean rosette casts during the whole experiment was found (Fig. 7a). DFe(II) and PFe(II) standing stocks were higher in fertilized waters while low in OUT stations independently of solar irradiance. On day 16, somewhat higher PFe(II) values were found under high irradiance at an OUT station but in conditions of higher than average Chl *a* concentrations at OUT stations. Thirdly, four days after the fertilization, samples of ML waters inside the fertilized patch collected at 3 different daytimes showed the same lack of dependence of DFe(II) on solar radiation (Fig. 7b). Finally, against the accepted paradigm and in agreement with our results, similar day and night time surface DFe(II) concentrations were also reported in ML waters of the Southern Ocean and the Pacific Ocean (Hansard et al., 2009; Sarthou et al., 2011), during the OIF SOIREE (Croot et al., 2001) and in estuarine waters (Hopwood et al., 2014).

The lack of correlation between Fe(II) concentrations and solar radiation does not imply that abiotic redox photoreactions involving colored DOM such as LMCT reactions (Blazevic et al., 2016) or abiotic superoxide generation (Rose, 2012) did not occur. During daytime, such reactions were certainly triggered, although we lack the necessary information to quantify their relevance. During the first week of the experiment, underway TLFe(II) concentrations seemed to be higher at daytime in fertilized as well as unfertilized areas (Fig. 6). However, this positive daytime effect was replaced by a strong relationship between TLFe(II) concentrations and biological parameters for the rest of the experiment (Table 3). To this respect, it is essential to remark that the activation of photoreactions in oxygen saturated waters implies that abiotic oxidative routes of Fe(II), forced by the photo-formation of reactive oxygen species (ROS) such as H_2O_2, O_2^- and OH· increase during daytime (Santana-Casiano et al., 2006).

Another process that could contribute to decrease daytime Fe(II) concentrations in the euphotic layer would be the photodegradation of Fe(II) ligands that delay the dark oxidation of Fe(II).

From a qualitative standpoint, solar radiation-dependent reactions are wavelength-dependent and usually show an exponential decay to

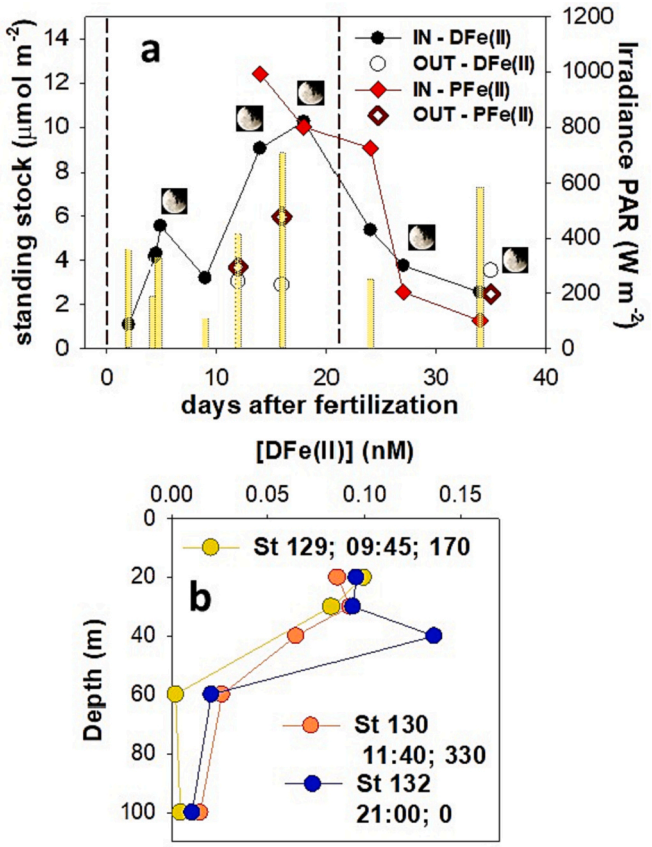

Fig. 7. a) Temporal evolution of dissolved (<0.2 mm) and particulate iron(II) standing stocks in fertilized (closed symbols) and non-fertilized (open symbols) waters measured during LOHAFEX and integrated over the upper 60 m of the water column. The two vertical dashed lines indicate the two fertilization events. The solar radiation registered at the end of each cast is indicated by a yellow bar. Night casts are indicated by the moon symbol. The maximum extent of the y-axis corresponds to the maximum irradiance measured at midday during LOHAFEX. b) DFe(II) vertical profiles measured on day 4 inside the fertilized patch at different times and solar irradiances. The legend indicates: station number; sampling time; GLOBAL solar irradiance (W m^{-2}). (For interpretation of the references to color in this figure legend, the reader is referred to the web version of this article.)

negligible values in the upper ~10–50 m following vertical light attenuation (Hansard et al., 2010; Laglera and van den Berg, 2007; Rijkenberg et al., 2004). The flat shape of all DFe(II) and PFe(II) profiles in the upper 50 m (Fig. 2) together with the similar concentrations found in underway samples are additional indications that photoreduction was not dominant throughout LOHAFEX.

Finally, the impact of LMCT reactions is also modulated by biota since photoreactions are strongly dependent on the nature of ligands (Barbeau et al., 2003; Rijkenberg et al., 2006). The substantial increase of the concentration of biological ligands during LOHAFEX could have changed their role Fe(III) photoreduction (Fig. 3e). The reduction of Fe (III) by superoxide in sunlit waters is also modulated by the organic and inorganic speciation of iron (Harrington and Crumbliss, 2009; Xing et al., 2019).

3.9. The effect of phytoplankton biomass and phagotrophy

During LOHAFEX, phytoplankton biomass (from Chl *a*), F_V/F_M and the concentration of iron in large copepod fecal pellets increased only in fertilized waters, while no marked changes were observed in community composition (Schulz et al., 2018).

Chl *a*, DFe(II) and PFe(II) showed low vertical variability in the upper 50 m followed by a sharp decrease down to 70 m depth and low concentrations in deeper waters (Fig. 2). The rise of DFe(II) and PFe(II) concentrations in the ML was strongly coupled to the increase of Chl *a* concentrations during the *growth* and *grazing* phases (Fig. 3). However, Chl *a* concentrations remained high during the *dilution* stage while both Fe(II) and PFe(II) concentrations decreased back to their initial values (Fig. 3). Despite this divergence, Chl *a* and DFe(II) as well as PFe(II) correlated significantly (Pearson correlation coefficients of 0.59, $p < 0.001$, $n = 71$ and 0.65, $p < 0.001$, $n = 53$ for Chl *a* vs DFe(II) and Chl *a* vs PFe(II), respectively).

In sunlit waters, unicellular organisms promote DFe(II) formation via ligand release contributing to photoreactions such as LMCT (Rijkenberg et al., 2006) and biological superoxide generation (Steigenberger et al., 2010; Wang et al., 2017). The increase of ligand concentrations during the first half of the experiment could have contributed to the concomitant increase of DFe(II) but their persistence until the end of the experiment (Fig. 3e) is at odds with the ~6-fold decrease of DFe(II) concentrations during the *dilution* stage (Fig. 3b).

Biological dark Fe(III) reduction processes could have contributed to higher night time DFe(II) concentrations (Fig. 5) as many unicellular marine organisms, including flagellates (in particular dinoflagellates) the dominant phyto- and zooplankton during LOHAFEX, are known to release reductant organics and/or produce superoxide (Aguirre et al., 2005; Sutherland et al., 2020). Dark reduction of Fe(III) in seawater has been confirmed in the presence of a range of planktonic groups: diatoms (Maldonado and Price, 2000; Maldonado and Price, 2001; Rijkenberg et al., 2008; Shaked et al., 2005), cyanobacteria (Rose et al., 2008) and bacteria (Henry and Vignais, 1980).

An important percentage of the flagellates found during LOHAFEX inside and outside the patch were most likely mixotrophs (Schulz et al., 2018), which implies phagotrophy. In the presence of high concentrations of colloidal iron and iron rich bacteria, flagellates accumulate high concentrations of iron via phagotrophy (Maranger et al., 1998). This process intervened in the fast accumulation of iron in copepod fecal pellets during LOHAFEX (Laglera et al., 2017). Animal cells release superoxide during phagocytosis (Babior, 1978) but this process still has to be studied in detail in marine organisms. As a response to phagotrophy, different algae may generate high levels of extracellular superoxide that would interfere with the process of prey-cell biorecognition (Martel, 2009). Moreover, day to night TLFe(II) differences could have been modulated by the diel feeding cycles characteristic of flagellates (Arias et al., 2020). However, flagellate phagotrophy could have contributed overall to increase Fe(II) oxidation rates in sunlit waters since maximum feeding is associated to ROS release (Diaz and Plummer, 2018) during daytime (Ng and Liu, 2016).

PFe(II) accumulation in fertilized waters could have been also driven by adsorption onto cell surfaces of dark-formed DFe(II) and reduction of adsorbed Fe(III) by superoxide formed in the dark. Further, different ferric binding groups and reductases located at the surface of many eukaryotic cells could also generate locally Fe(II) to facilitate iron uptake (Morrissey and Bowler, 2012).

A barely studied topic is the existence of a diel cycle in iron uptake that would certainly affect ocean surface day to night DFe(II) concentrations. Large diurnal variations in cellular iron content have been observed in *Crocosphaera watsonii*, a single-celled diazotrophic cyanobacteria (Tuit et al., 2004). However, N_2-fixing is not a relevant process in the nitrate rich Southern Ocean including the LOHAFEX area. To the best of our knowledge, there has been no similar study for flagellate species.

3.10. The role of copepod grazing and F_V/F_M ratios

The abundance of large copepods in the ML (due to vertical migration) and photosynthesis rate were the main biological variables showing a strong daily cycle (Laglera et al., 2017; Martin et al., 2013; Mazzocchi et al., 2009; Schulz et al., 2018). Since Fe(II) is an important

component of intracellular Fe, sloppy feeding during copepod grazing should also be considered a potential source of DFe(II) to the surface ocean. During LOHAFEX, sloppy feeding and coprophagy by large copepods were important in the cycling of DFe and dissolved iron ligands (Laglera et al., 2017; Laglera et al., 2020; Martin et al., 2013). Although prior incubation experiments with large copepod grazing on diatoms showed no Fe(II) increase (Hopwood et al., 2020), during LOHAFEX, DFe(II) was an important fraction of the rapidly taken up and recycled DFe (Fig. 3G). Daytime migration of large copepods well below the ML (Mazzocchi et al., 2009) rules out any possible grazing-driven daytime spill of Fe(II) in the ML but could explain the higher nighttime TLFe(II) concentrations (Figs. 5 and 6). Our results point to the possibility that complex trophic interactions could have controlled iron redox speciation in an assemblage akin to the nutrient limited regenerating systems (Smetacek and Pollehne, 1986) as typical bloom-forming diatom species represented only a minor component of the community inside fertilized waters.

During the *growth* and *grazing* stages of LOHAFEX, a concomitant increase and peaking of DFe(II) and ligands was found. During the *dilution* stage of the experiment, ligands decreased in the ML by about 20 % mostly due to the disappearance in the upper 50 m of the strong iron ligand L_1 (Fig. 3e) (Laglera et al., 2020). The temporal and spatial evolution of DFe(II) followed closely that of L_1. L_1 was absent before the initial fertilization, appeared during the *growth* stage, peaked during the *grazing* stage, and during the *dilution* stage remained high at depth but disappeared from the upper 50 m of the water column (Fig. 3H) (Laglera et al., 2020). Since L_1 concentrations went from below the detection limit to the nanomolar range, its presence could also explain the 6-fold increment of DFe(II) concentrations. Based on the strong correlation between DFe and L_1, it was proposed that DFe was mostly recycled as FeL_1 complexes due to sloppy feeding of phytoplankton and coprophagy by copepods (Laglera et al., 2020). Further, L_1 was possibly an intracellular photolabile iron ligand (pigment like) which would explain its photodegradation in sunlit waters (Laglera et al., 2020). Our DFe(II) results support this interpretation. Grazing would spill part of DFe in the specific form of Fe(*II*)L_1 complexes. In the ML, Fe(*II*)L_1 complexes would be involved in oxidation/reduction cycles before L_1 photodegradation or Fe(II) uptake. This photodegradation of stabilizing or promoting Fe(II) concentrations would also affect daytime vs nighttime Fe(II) ratios. Below the euphotic layer, L_1 would persist for longer contributing to the deep Fe(II) maximum and the abundant presence of L_1 below the ML (Fig. 3H).

The dependence of DFe(II) and L_1 on zooplankton grazing is at odds with the observations outside the patch where L_1 was found together with consistently lower DFe(II). The key parameter here, F_V/F_M, indicates that only in fertilized waters pigments in both photosystems were iron replete (we assume both photosystems although F_V/F_M only responds to photosystem II). Therefore, after the alleviation of iron limitation, phytoplankton contained not only more iron per cell in the fertilized patch but also more Fe(II) complexes (here with L_1).

As a summary we hypothesize that a combination of both, lower oxidizing ROS photogeneration and higher Fe(*II*)L_1 spill after sloppy feeding at night, would explain the temporal and spatial trends observed (Fig. 8).

3.11. The deep DFe(II), nitrite and ammonium maxima

Throughout LOHAFEX, and despite high oxygen concentrations (Fig. 1c), DFe(II), nitrite and ammonium accumulated below the ML in fertilized waters (Figs. 3 and 9). The nitrite and ammonium maxima were found below the ML at ~100 m depth with a deeper DFe(II) maximum at ~150 m depth. Our only vertical profile extending further down (300 m depth on day 14) indicates that the DFe(II) maximum was limited to the 100–150 m depth range. Higher prefertilization NO_2^- and NH_4^+ concentrations below the ML (Fig. 9) were caused by the rise and decline of a phytoplankton bloom prior to our arrival, as indicated by

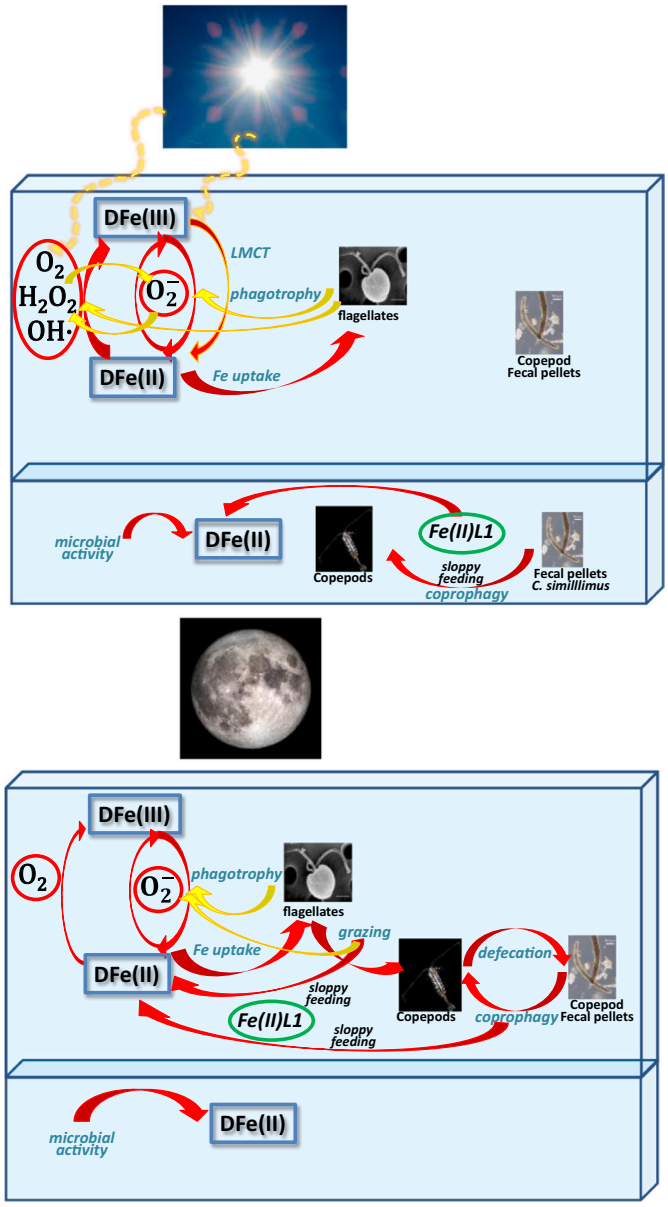

Fig. 8. Major processes affecting iron redox speciation at day and night in the upper 200 m of the water column during the LOHAFEX experiment. Iron redox species are enclosed in blue boxes. Oxygen species intervening in iron reduction and oxidation are enclosed in red circles. Red arrows indicate Fe fluxes, yellow arrows indicate transformation of oxygen species. Minor iron and oxygen fluxes are not shown in the interests of clarity. (For interpretation of the references to color in this figure legend, the reader is referred to the web version of this article.)

initial low Si concentrations (Schulz et al., 2018). Both nitrogen species reached background concentrations on day 4 and increased again reaching a maximum at the end of the experiment (Fig. 9). In the OUT stations, NO_2^- and NH_4^+ maxima were also found and data from day 16 (Fig. 3) suggests that a deep DFe(II) maximum was also formed in non-fertilized waters.

Deep DFe(II) maxima at or just below deep NO_2^- maxima have been described in the Arabian Sea (Kondo and Moffett, 2013; Moffett et al., 2007) and the tropical North Pacific (Hopkinson and Barbeau, 2007). Different authors suggested that denitrifiers would be responsible for the extracellular reduction of iron due to their high iron requirement. During LOHAFEX, however, oxygen concentrations were high during the whole cruise (Fig. 1c). A deep TLFe(II) maximum in the depth range

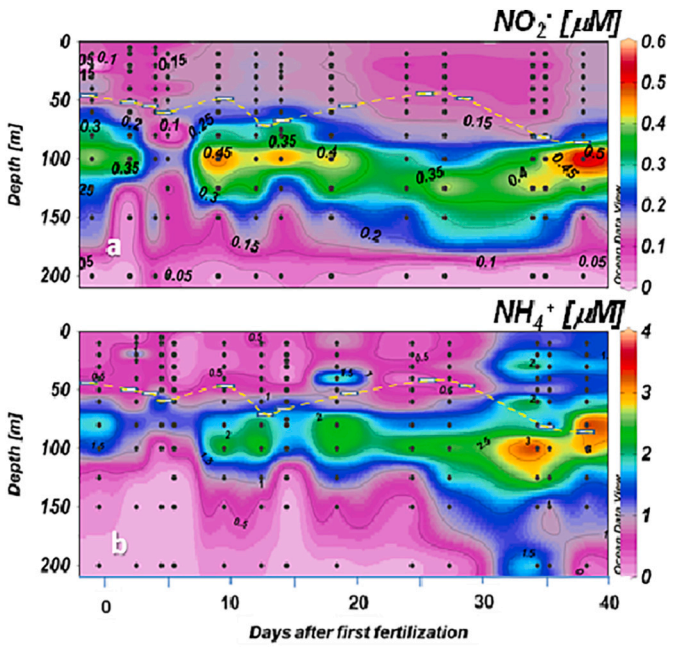

Fig. 9. Time course of nitrite and ammonium concentrations in the upper 200 m of the water column in fertilized waters during LOHAFEX. The dashed white line indicates the depth of the mixed layer (ML) deepening from ~40 m to 80 m and coincident with the lower limit of biomass accumulation.

of 90 to 300 m was found at several stations in a North to South transect across the oxygenated waters of the ACC in the eastern Atlantic sector of the Southern Ocean (Sarthou et al., 2011). Sarthou and coauthors hypothesized that the Fe(II) source was the remineralization and/or disaggregation of particles. NO_2^- and NH_4^+ deep maxima were also found in high latitude shelf waters of the Bering Sea (Mordy et al., 2010). Recent works not related to Fe(II), have suggested that NO_2^- concentrations below the euphotic layer are due to nitrifying organisms (Zakem et al., 2018). Interestingly, NH_4^+ oxidizing microbes seem to activate the extracellular reduction of Fe(III) for its later uptake (Shafiee et al., 2019).

In theory, high DFe(II) and NO_2^- concentrations in oxygenated waters should not co-occur since this would lead to chemodenitrification, i.e. the abiotically combined oxidation of DFe(II) and reduction of NO_2^- mostly to N_2O (Chen et al., 2020). Chemodenitrification could have been relevant below the ML during LOHAFEX, since it involves the oxidation of adsorbed Fe(II), explaining the negligible PFe(II) concentrations found in deeper layers. Since NO_2^- is not fully converted to N_2O (Chen et al., 2020) and the nitrogen species that would close the mass balance was not identified by Chen and coauthors, we hypothesize that during LOHAFEX the imbalance could be caused by the formation of NH_4^+.

We have argued before that the spatial and temporal patchiness of DFe and mainly L and L_1 below the ML depth was due to sloppy feeding and coprophagy. The large reduction of fecal pellet concentrations in the depth range from 40 to 200 m would support this (Laglera et al., 2017). Further, the grazing activity leads to excretion of NH_4^+ down to at least 150 m (as indicated by L_1 found down to 200 m), the daily migration range of copepods during LOHAFEX (Martin et al., 2013; Mazzocchi et al., 2009). In the ML, NH_4^+ would be quickly taken up but would activate the action of ammonium oxidizers below that (Valdés et al., 2018) explaining the local high NO_2^- and DFe(II) concentrations (Shafiee et al., 2019). Abiotic chemodenitrification would prevent the accumulation of high NO_2^- and Fe(II) concentrations. During the *dilution* stage, the relaxation, to some extent, of the activity of primary producers and grazers (zero NCP in decreasing Chl *a* concentrations) would explain the appearance of NH_4^+ in the ML and the late peak in NO_2^- concentrations. Therefore, the combination of abiotic and biological processes mentioned above could account for the vertical distribution and temporal evolution of DFe(II), NO_2^- and NH_4^+ throughout LOHAFEX.

4. Conclusions

Despite the recognized importance of Fe(II) for primary production and biogeochemical processes in the world's oceans, its cycling is poorly understood.

The LOHAFEX experiment gave an invaluable opportunity to study and follow the iron redox speciation in a watermass with a stable plankton assemblage composition and without the caveats of significant vertical or horizontal inputs. LOHAFEX biogeochemical conditions were quite simple if compared to the spatial and temporal evolution of biogeochemical parameters during previous fertilization experiments and the complex composition of many other Antarctic biological communities. We want to remark that further investigation is necessary in order to export our methodologies and apply our conclusions to other marine environments.

Our data shows, for the first time, that sample filtration removes an important fraction of the chemiluminescence signal from surface oceanic samples, suggesting that particle surfaces are important contributors to Fe(II) concentrations in the ocean. We found 6-fold rise and fall of DFe(II) and PFe(II) concentrations in the mixed layer limited to fertilized waters with a lack of relationship to solar radiation. This pattern together with the strong relation between DFe(II) concentrations and plankton biomass is only possible if biological processes have a strong control of iron redox speciation.

While we could not directly characterize PFe(II), the main contribution seemed to be Fe(II) adsorbed to biological surfaces. Future work should address the description of the nature of cellular surface Fe(II) binding groups and Fe(II) fluxes between the particulate and dissolved fractions.

Our findings about iron redox chemistry in this work fit the conceptual framework published about Fe(II+III) cycling during LOHAFEX based on a biological control of iron concentrations and speciation. We propose that during LOHAFEX the release of intracellular Fe(II)-L_1 complexes during sloppy feeding on iron-replenished cells and fecal pellets by large copepods was the main source of the higher DFe(II) concentrations in fertilized waters. This process explains both the higher concentrations at night in the ML and the presence of DFe(II) below the euphotic layer. The lack of Fe(II) oxidation at low DFe(II) concentrations but complete oxidation after extra addition of 2.5 nM Fe(II) indicate that specific Fe(II) ligands (L_1 and possibly others) controlled DFe(II) concentrations. Formation of Fe(II) was possibly countered during daytime by ROS released during feeding by phagotrophic flagellates as well as other ROS formation reactions involving irradiation of DOM. We argue that biological processes could even exert a top down control on iron redox speciation.

During LOHAFEX we also found a deep Fe(II) maximum coincident with nitrite and ammonium maxima. We suggest that, under oxygen saturation, high values of deep Fe(II) can be also caused by sloppy feeding of copepods on sinking fecal pellets. Concentrations of reduced species would have been controlled by the action of copepod excretion, ammonium oxidizing, nitrifying microbes, and chemodenitrification during LOHAFEX.

CRediT authorship contribution statement

Luis M. Laglera: Writing – original draft, Conceptualization, Methodology, Funding acquisition. **Hema Uskaikar:** Formal analysis. **Christine Klaas:** Formal analysis, Writing – review & editing. **S. Wajih A. Naqvi:** Writing – review & editing, Project administration. **Dieter A. Wolf-Gladrow:** Writing – review & editing. **Antonio Tovar-Sánchez:** Funding acquisition, Project administration, Writing – review & editing.

Declaration of competing interest

The authors declare that they have no known competing financial interests or personal relationships that could have appeared to influence the work reported in this paper.

Data availability

All Fe(II) data used for this article can be found a the Pangaea repository: https://doi.org/10.1594/PANGAEA.926118 and https://doi.org/10.1594/PANGAEA.926101

Acknowledgments

We are grateful to Captain Stefan Schwarze and the crew of the RV Polarstern. All the members of the LOHAFEX community contributed to this work via discussion during the cruise and subsequent workshops.

Funding

This work was funded by the Spanish Government via MINECO (CTM2008-880 01864-E/ANT, CTM2014-59244-C3-3-R) and MCIN/AEI/10.13039/501100011033 (PID2020-115291GB-I00) projects.

Appendix A. Supplementary data

Supplementary data to this article can be found online at https://doi.org/10.1016/j.marpolbul.2022.114161.

References

Aguirre, J., Ríos-Momberg, M., Hewitt, D., Hansberg, W., 2005. Reactive oxygen species and development in microbial eukaryotes. Trends Microbiol. 13 (3), 111–118.
Anderson, R.F., Mawji, E., Cutter, G.A., Measures, C.I., Jeandel, C., 2014. GEOTRACES Changing the Way We Explore Ocean Chemistry. Oceanography 27 (1), 50–61.
Arias, A., Saiz, E., Calbet, A., 2020. Towards an understanding of diel feeding rhythms in marine protists: consequences of light manipulation. Microb. Ecol. 79 (1), 64–72.
Arreguin, M.L., et al., 2021. The role of gentisic acid on the Fe(III) redox chemistry in marine environments. Mar. Chem. 234, 104003.
Assmy, P., Henjes, J., Klaas, C., Smetacek, V., 2007. Mechanisms determining species dominance in a phytoplankton bloom induced by the iron fertilization experiment EisenEx in the Southern Ocean. Deep-Sea Res. I Oceanogr. Res. Pap. 54 (3), 340–362.
Babior, B.M., 1978. Oxygen-dependent microbial killing by phagocytes. N. Engl. J. Med. 298 (12), 659–668.
Barbeau, K., Rue, E.L., Trick, C.G., Bruland, K.W., Butler, A., 2003. Photochemical reactivity of siderophores produced by marine heterotrophic bacteria and cyanobacteria based on characteristic Fe(III) binding groups. Limnol. Oceanogr. 48 (3), 1069–1078.
Blazevic, A., et al., 2016. Photoreduction of terrigenous Fe-humic substances leads to bioavailable iron in oceans. Angew. Chem. 128 (22), 6527–6532.
Bligh, M.W., Waite, T.D., 2011. Formation, reactivity, and aging of ferric oxide particles formed from Fe(II) and Fe(III) sources: implications for iron bioavailability in the marine environment. Geochim. Cosmochim. Acta 75 (24), 7741–7758.
Bolster, K., Heller, M., Moffett, J., 2018. Determination of iron (II) by chemiluminescence using masking ligands to distinguish interferences. Limnol. Oceanogr. Methods 16 (11), 750–759.
Bowie, A.R., Achterberg, E.P., Sedwick, P.N., Ussher, S., Worsfold, P.J., 2002. Real-time monitoring of picomolar concentrations of iron(II) in marine waters using automated flow injection-chemiluminescence instrumentation. Environ. Sci. Technol. 36 (21), 4600–4607.
Chen, D., et al., 2020. Chemodenitrification by Fe(II) and nitrite: pH effect, mineralization and kinetic modeling. Chem. Geol. 541, 119586.
Cooper, D.J., Watson, A.J., Nightingale, P.D., 1996. Large decrease in ocean-surface CO2 fugacity in response to in situ iron fertilization. Nature 383, 511–513.
Croot, P.L., Laan, P., 2002. Continuous shipboard determination of Fe(II) in polar waters using flow injection analysis with chemiluminescence detection. Anal. Chim. Acta 466 (2), 261–273.
Croot, P.L., et al., 2001. Retention of dissolved iron and Fe II in an iron induced Southern Ocean phytoplankton bloom. Geophys. Res. Lett. 28 (18), 3425–3428.
Croot, P.L., et al., 2005. Spatial and temporal distribution of Fe(II) and H2O2 during EisenEx, an open ocean mescoscale iron enrichment. Mar. Chem. 95 (1–2), 65–88.
Croot, P.L., et al., 2008. Regeneration of Fe(II) during EIFeX and SOFeX. Geophys. Res. Lett. 35 (19).
Diaz, J.M., Plummer, S., 2018. Production of extracellular reactive oxygen species by phytoplankton: past and future directions. J. Plankton Res. 40 (6), 655–666.
Ebersbach, F., et al., 2014. Particle flux characterisation and sedimentation patterns of protistan plankton during the iron fertilisation experiment LOHAFEX in the Southern Ocean. Deep-Sea Res. I Oceanogr. Res. Pap. 89, 94–103.
Gonzalez, H.E., Smetacek, V., 1994. The possible role of the cyclopoid copepod Oithona in retarding vertical flux of zooplankton faecal material. Mar. Ecol. Prog. Ser. 113 (3), 233–246.
González, A.G., Santana-Casiano, J.M., González-Davila, M., Pérez, N., 2012. Effect of organic exudates of Phaeodactylum tricornutum on the Fe (II) oxidation rate constant Efecto de los exudados orgánicos de Phaeodactylum tricornutum en la constante de velocidad de oxidación del Fe (II). Cienc. Mar. 38 (1B), 245–261.
González, A.G., Santana-Casiano, J.M., González-Dávila, M., Pérez-Almeida, N., Suárez de Tangil, M., 2014. Effect of Dunaliella tertiolecta organic exudates on the Fe(II) oxidation kinetics in seawater. Environ.Sci.Technol. 48 (14), 7933–7941.
González, A.G., Cadena-Aizaga, M.I., Sarthou, G., González-Dávila, M., Santana-Casiano, J.M., 2019. Iron complexation by phenolic ligands in seawater. Chem. Geol. 511, 380–388.
Gonzalez-Davila, M., Santana-Casiano, J.M., Millero, F.J., 2005. Oxidation of iron(II) nanomolar with H2O2 in seawater. Geochim. Cosmochim. Acta 69 (1), 83–93.
Haddock, S.H.D., Moline, M.A., Case, J.F., 2010. Bioluminescence in the sea. Annu. Rev. Mar. Sci. 2 (1), 443–493.
Hansard, S.P., Landing, W.M., Measures, C.I., Voelker, B.M., 2009. Dissolved iron(II) in the Pacific Ocean: measurements from the PO2 and P16N CLIVAR/CO2 repeat hydrography expeditions. Deep-Sea Res. I Oceanogr. Res. Pap. 56 (7), 1117–1129.
Hansard, P.S., Vermilyea, A.W., Voelker, B.M., 2010. Measurements of superoxide radical concentration and decay kinetics in the Gulf of Alaska. Deep-Sea Res. I Oceanogr. Res. Pap. 57 (9), 1111–1119.
Harrington, J.M., Crumbliss, A.L., 2009. The redox hypothesis in siderophore-mediated iron uptake. Biometals 22 (4), 679–689.
Heller, M.I., Croot, P.L., 2010. Superoxide decay kinetics in the Southern Ocean. Environ. Sci. Technol. 44 (1), 191–196.
Henry, M.F., Vignais, P.M., 1980. Production of superoxide anions in Paracoccus denitrificans. Arch. Biochem. Biophys. 203 (1), 365–371.
Hopkinson, B.M., Barbeau, K.A., 2007. Organic and redox speciation of iron in the eastern tropical North Pacific suboxic zone. Mar. Chem. 106, 2–17.
Hopwood, M.J., Statham, P.J., Milani, A., 2014. Dissolved Fe(II) in a river-estuary system rich in dissolved organic matter. Estuar. Coast. Shelf Sci. 151, 1–9.
Hopwood, M.J., et al., 2017. A comparison between four analytical methods for the measurement of Fe(II) at nanomolar concentrations in coastal seawater. Front. Mar. Sci. 4 (JUN).
Hopwood, M.J., et al., 2020. Fe(II) stability in coastal seawater during experiments in Patagonia, Svalbard, and Gran Canaria. Biogeosciences 17 (5), 1327–1342.
Iversen, M.H., Poulsen, L.K., 2007. Coprorhexy, coprophagy, and coprochaly in the copepods Calanus helgolandicus, Pseudocalanus elongatus, and Oithona similis. Mar. Ecol. Prog. Ser. 350, 79–89.
King, D.W., Lounsbury, H.A., Millero, F.J., 1995. Rates and mechanism of Fe(II) oxidation at nanomolar total iron concentrations. Environmental Science & Technology 29, 818–824.
Kolber, Z.S., et al., 1994. Iron limitation of phytoplankton photosynthesis in the equatorial Pacific Ocean. Nature 371, 145–149.
Kondo, Y., Moffett, J.W., 2013. Dissolved Fe(II) in the Arabian Sea oxygen minimum zone and western tropical Indian Ocean during the inter-monsoon period. Deep-Sea Res. I Oceanogr. Res. Pap. 73, 73–83.
Laglera, L.M., van den Berg, C.M.G., 2007. Wavelength dependence of the photochemical reduction of iron in arctic seawater. Environ. Sci. Technol. 41 (7), 2296–2302.
Laglera, L.M., Battaglia, G., van den Berg, C.M.G., 2011. Effect of humic substances on the iron speciation in natural waters by CLE/CSV. Mar. Chem. 127 (1–4), 134–143.
Laglera, L.M., Santos-Echeandía, J., Caprara, S., Monticelli, D., 2013. Quantification of iron in seawater at the low picomolar range based on optimization of bromate/ammonia/dihydroxynaphtalene system by catalytic adsorptive cathodic stripping voltammetry. Anal. Chem. 85 (4), 2486–2492.
Laglera, L.M., et al., 2017. Iron partitioning during LOHAFEX: copepod grazing as a major driver for iron recycling in the Southern Ocean. Mar. Chem. 196, 148–161.
Laglera, L.M., et al., 2020. Iron organic speciation during the LOHAFEX experiment: iron ligands release under biomass control by copepod grazing. J. Mar. Syst. 207, 103151.
Lee, Y.P., Fujii, M., Kikuchi, T., Terao, K., Yoshimura, C., 2017. Variation of iron redox kinetics and its relation with molecular composition of standard humic substances at circumneutral pH. PloS one 12 (4), e0176484.
Liu, X.W., Millero, F.J., 2002. The solubility of iron in seawater. Mar. Chem. 77 (1), 43–54.
Lohan, M.C., Bruland, K.W., 2008. Elevated Fe(II) and dissolved Fe in hypoxic shelf waters off Oregon and Washington: an enhanced source of iron to coastal upwelling regimes. Environ. Sci. Technol. 42 (17), 6462–6468.
Maldonado, E.M., Latz, M.I., 2007. Shear-stress dependence of dinoflagellate bioluminescence. Biol. Bull. 212 (3), 242–249.
Maldonado, M.T., Price, N.M., 2000. Nitrate regulation of Fe reduction and transport by Fe-limited Thalassiosira oceanica. Limnol. Oceanogr. 45 (4), 814–826.
Maldonado, M.T., Price, N.M., 2001. Reduction and transport of organically bound iron by Thalassiosira oceanica (Bacillariophyceae). J. Phycol. 37 (2), 298–310.
Maldonado, M.T., et al., 2001. Iron uptake and physiological response of phytoplankton during a mesoscale Southern Ocean iron enrichment. Limnol. Oceanogr. 46 (7), 1802–1808.
Maranger, R., Bird, D.F., Price, N.M., 1998. Iron acquisition by photosynthetic marine phytoplankton from ingested bacteria. Nature 396, 248–251.

Martel, C.M., 2009. Conceptual bases for prey biorecognition and feeding selectivity in the microplanktonic marine phagotroph Oxyrrhis marina. Microb. Ecol. 57 (4), 589–597.
Martin, P., et al., 2013. Iron fertilization enhanced net community production but not downward particle flux during the Southern Ocean iron fertilization experiment LOHAFEX. Glob. Biogeochem. Cycles 27 (3), 871–881.
Mazzocchi, M.G., et al., 2009. A non-diatom plankton bloom controlled by copepod grazing and amphipod predation: preliminary results from the LOHAFEX iron-fertilisation experiment. GLOBEC Int. Newsl. (15), 3–6.
Melnik, A., Melnik, L., Mashukova, O., Melnikov, V., 2021. Field studies of bioluminescence in the Antarctic sector of the Atlantic Ocean in 2002 and 2020. Luminescence 36 (8), 1910–1921.
Moffett, J.W., Goeffert, T.J., Naqvi, S.W.A., 2007. Reduced iron associated with secondary nitrite maxima in the Arabian Sea. Deep-Sea Res. I Oceanogr. Res. Pap. 54 (8), 1341–1349.
Møller, E.F., Thor, P., Nielsen, T.G., 2003. Production of DOC by Calanus finmarchicus, C. glacialis and C. hyperboreus through sloppy feeding and leakage from fecal pellets. Mar. Ecol. Prog. Ser. 262, 185–191.
Moore, J., Braucher, O., 2008. Sedimentary and mineral dust sources of dissolved iron to the world ocean. Biogeosciences 5, 631–656.
Mordy, C.W., et al., 2010. Temporary uncoupling of the marine nitrogen cycle: accumulation of nitrite on the Bering Sea shelf. Mar. Chem. 121 (1), 157–166.
Morrissey, J., Bowler, C., 2012. Iron utilization in marine cyanobacteria and eukaryotic algae. Front. Microbiol. 3.
Murchie, E.H., Lawson, T., 2013. Chlorophyll fluorescence analysis: a guide to good practice and understanding some new applications. J. Exp. Bot. 64 (13), 3983–3998.
Ng, W.H.A., Liu, H., 2016. Diel periodicity of grazing by heterotrophic nanoflagellates influenced by prey cell properties and intrinsic grazing rhythm. J. Plankton Res. 38 (3), 636–651.
Noji, T.T., Estep, K.W., Macintyre, F., Norrbin, F., 1991. Image analysis of faecal material grazed upon by three species of copepods: evidence for coprorhexy, coprophagy and coprochaly. J. Mar. Biol. Assoc. U. K. 71 (02), 465–480.
Pérez-Almeida, N., González, A.G., Santana-Casiano, J.M., González-Dávila, M., 2022. Ocean acidification effect on the iron-gallic acid redox interaction in seawater. Front. Mar. Sci. 9, 837363.
Pollard, R.T., et al., 2009. Southern Ocean deep-water carbon export enhanced by natural iron fertilization. Nature 457 (7229), 577–580.
Rijkenberg, M.J.A., et al., 2004. UVA variability overrules UVB ozone depletion effects on the photoreduction of iron in the Southern Ocean. Geophys. Res. Lett. 31 (24).
Rijkenberg, M.J.A., et al., 2005. The influence of UV irradiation on the photoreduction of iron in the Southern Ocean. Mar. Chem. 93 (2–4), 119–129.
Rijkenberg, M.J.A., Gerringa, L.J.A., Carolus, V.E., Velzeboer, I., de Baar, H.J.W., 2006. Enhancement and inhibition of iron photoreduction by individual ligands in open ocean seawater. Geochim. Cosmochim. Acta 70 (11), 2790–2805.
Rijkenberg, M.J.A., et al., 2008. Changes in iron speciation following a Saharan dust event in the tropical North Atlantic Ocean. Mar. Chem. 110 (1–2), 56–67.
Rose, A.L., 2012. The influence of extracellular superoxide on iron redox chemistry and bioavailability to aquatic microorganisms. Front. Microbiol. 3 (APR).
Rose, A.L., Waite, T.D., 2001. Chemiluminescence of luminol in the presence of iron(II) and oxygen: oxidation mechanism and implications for its analytical use. Anal. Chem. 73 (24), 5909–5920.
Rose, A.L., Waite, T.D., 2002. Kinetic model for Fe(II) oxidation in seawater in the absence and presence of natural organic matter. Environ. Sci. Technol. 36 (3), 433–444.
Rose, A.L., Waite, T.D., 2003a. Effect of dissolved natural organic matter on the kinetics of ferrous iron oxygenation in seawater. Environ.Sci.Technol. 37 (21), 4877–4886.
Rose, A.L., Waite, T.D., 2003b. Predicting iron speciation in coastal waters from the kinetics of sunlight-mediated iron redox cycling. Aquat. Sci. 65 (4), 375–383.
Rose, A.L., Waite, T.D., 2005. Reduction of organically complexed ferric iron by superoxide in a simulated natural water. Environ.Sci.Technol. 39 (8), 2645–2650.
Rose, A.L., Webb, E.A., Waite, T.D., Moffett, J.W., 2008. Measurement and implications of nonphotochemically generated superoxide in the equatorial Pacific Ocean. Environ.Sci.Technol. 42 (7), 2387–2393.
Roy, E.G., Wells, M.L., King, D.W., 2008. Persistence of iron(II) in surface waters of the western subarctic Pacific. Limnol. Oceanogr. 53 (1), 89–98.
Santana-Casiano, J.M., Gonzalez-Davila, M., Rodriguez, M.J., Millero, F.J., 2000. The effect of organic compounds in the oxidation kinetics of Fe(II). Mar. Chem. 70 (1–3), 211–222.
Santana-Casiano, J.M., González-Dávila, M., Millero, F.J., 2006. The role of Fe(II) species on the oxidation of Fe(II) in natural waters in the presence of O2 and H2O2. Mar. Chem. 99 (1–4), 70–82.
Santana-González, C., et al., 2018. Fe(II) oxidation kinetics in the North Atlantic along the 59.5° N during 2016. Mar. Chem. 203, 64–77.
Santana-González, C., González-Dávila, M., Santana-Casiano, J.M., Gladyshev, S., Sokov, A., 2019. Organic matter effect on Fe(II) oxidation kinetics in the Labrador Sea. Chem. Geol. 511, 238–255.
Sarthou, G., et al., 2011. Labile Fe(II) concentrations in the Atlantic sector of the Southern Ocean along a transect from the subtropical domain to the Weddell Sea Gyre. Biogeosciences 8 (9), 2461–2479.
Schlosser, C., et al., 2018. H2S events in the Peruvian oxygen minimum zone facilitate enhanced dissolved Fe concentrations. Sci. Rep. 8 (1), 12642.
Schulz, I., et al., 2018. Remarkable structural resistance of a nanoflagellate-dominated plankton community to iron fertilization during the Southern Ocean experiment LOHAFEX. Mar. Ecol. Prog. Ser. 601, 77–95.
Shafiee, R.T., Snow, J.T., Zhang, Q., Rickaby, R.E.M., 2019. Iron requirements and uptake strategies of the globally abundant marine ammonia-oxidising archaeon, Nitrosopumilus maritimus SCM1. ISME J. 13 (9), 2295–2305.
Shaked, Y., 2008. Iron redox dynamics in the surface waters of the Gulf of Aqaba,Red Sea. Geochim. Cosmochim. Acta 72 (6), 1540–1554.
Shaked, Y., Rose, A., 2013. Seas of superoxide. Science 340 (6137), 1176–1177.
Shaked, Y., Kustka, A.B., Morel, F.M.M., 2005. A general kinetic model for iron acquisition by eukaryotic phytoplankton. Limnol. Oceanogr. 50 (3), 872–882.
Singh, S.K., et al., 2015. Response of bacterioplankton to iron fertilization of the Southern Ocean,Antarctica. Front. Microbiol. 6 (863).
Smetacek, V., Naqvi, S.W.A., 2010. The Expedition of the Research Vessel "Polarstern" to the Antarctic in 2009 (ANT-XXV/3 - LOHAFEX). Alfred-Wegener-Institut für Polar- und Meeresforschung, Bremerhaven.
Smetacek, V., Pollehne, F., 1986. Nutrient cycling in pelagic systems: a reappraisal of the conceptual framework. Ophelia 26 (1), 401–428.
Steigenberger, S., Statham, P.J., Völker, C., Passow, U., 2010. The role of polysaccharides and diatom exudates in the redox cycling of Fe and the photoproduction of hydrogen peroxide in coastal seawaters. Biogeosciences 7 (1), 109–119.
Stumm, W., Morgan, J., 1996. Aquatic Chemistry: Chemical Equilibria and Rates in Natural Waters, third edition. Wiley, New York [ua].
Sutherland, K.M., Wankel, S.D., Hansel, C.M., 2020. Dark biological superoxide production as a significant flux and sink of marine dissolved oxygen. Proc. Natl. Acad. Sci. 117 (7), 3433–3439.
Thiele, S., Fuchs, B.M., Ramaiah, N., Amanna, R., 2012. Microbial community response during the iron fertilization experiment LOHAFEX. Appl. Environ. Microbiol. 78 (24), 8803–8812.
Thiele, S., et al., 2014. Stable composition of the nano- and picoplankton community during the ocean iron fertilization experiment LOHAFEX. PLoS ONE 9 (11), e113244.
Tovar-Sánchez, A., 2012. Sampling approaches for trace elements determination in seawater. In: Pawliszyn, J. (Ed.), Comprehensive Sampling and Sample Preparation: Analytical Techniques for Scientists. Academic Press Elsevier, New York, pp. 317–334.
Tovar-Sanchez, A., et al., 2003. A trace metal clean reagent to remove surface-bound iron from marine phytoplankton. Mar. Chem. 82 (1–2), 91–99.
Tuit, C., Waterbury, J., Ravizza, G., 2004. Diel variation of molybdenum and iron in marine diazotrophic cyanobacteria. Limnol. Oceanogr. 49 (4), 978–990.
Ussher, S.J., Yaqoob, M., Achterberg, E.P., Nabi, A., Worsfold, P.J., 2005. Effect of model ligands on iron redox speciation in natural waters using flow injection with luminol chemiluminescence detection. Anal. Chem. 77 (7), 1971–1978.
Ussher, S.J., et al., 2009. Investigation of iron(III) reduction and trace metal interferences in the determination of dissolved iron in seawater using flow injection with luminol chemiluminescence detection. Anal. Chim. Acta 652 (1–2), 259–265.
Valdés, V., Fernandez, C., Molina, V., Escribano, R., 2018. Nitrogen excretion by copepods and its effect on ammonia-oxidizing communities from a coastal upwelling zone. Limnol. Oceanogr. 63 (1), 278–294.
van den Berg, C.M.G., 2006. Chemical speciation of iron in seawater by cathodic stripping voltammetry with dihydroxynaphthalene. Anal. Chem. 78 (1), 156–163.
von der Heyden, B.P., et al., 2014. Ubiquitous presence of Fe(II) in aquatic colloids and its association with organic carbon. Environ.Sci.Technol.Lett. 1 (10), 387–392.
Waite, T.D., Szymczak, R., Espey, Q.I., Furnas, M.J., 1995. Diel variations in iron speciation in northern australian shelf waters. Mar. Chem. 50 (1–4), 79–91.
Wang, K., Garg, S., Waite, T.D., 2017. Light-mediated reactive oxygen species generation and iron redox transformations in the presence of exudate from the cyanobacterium Microcystis aeruginosa. Environ.Sci.Technol. 51 (15), 8384–8395.
Wells, M.L., Mayer, L.M., Donard, O.F.X., De Souza Sierra, M.M., Ackelson, S.G., 1991. The photolysis of colloidal iron in the oceans. Nature 353 (6341), 248–250.
Xing, G., Garg, S., Waite, T.D., 2019. Is superoxide-mediated Fe(III) reduction important in sunlit surface waters? Environ.Sci.Technol. 53 (22), 13179–13190.
Zakem, E.J., et al., 2018. Ecological control of nitrite in the upper ocean. Nat. Commun. 9 (1), 1206.